2009

INVESTIGATION OF THE MECHANICAL PROPERTIES OF POLY (ETHYLENE GLYCOL) DIACRYLATE BY NANOINDENTATION USING ATOMIC FORCE MICROSCOPY

Zouheir Drira
Virginia Commonwealth University

INVESTIGATION OF THE MECHANICAL PROPERTIES OF POLY (ETHYLENE GLYCOL) DIACRYLATE BY NANOINDENTATION USING ATOMIC FORCE MICROSCOPY

A thesis submitted in partial fulfillment of the requirements for the degree of Master of Science in Chemical and Life Engineering at Virginia Commonwealth University

By

Zouheir Drira
B.S. Murray State University, December 2006

Advisor: Dr. Vamsi K Yadavalli,
Assistant Professor, Chemical and Life Engineering

Virginia Commonwealth University
Richmond, Virginia
December, 2009

Acknowledgments

I would like to thanks my research advisor, Dr. Vamsi Yadavalli for his patience, direction and support over the course of this research. He was a constant inspiration, and his assistance and suggestions were invaluable towards the completion of this work.

I would also like to thank the members of my exam committee, Dr. Stephen Fong and Dr. Gary Bowlin for their efforts in reviewing and evaluating my research. I would like to acknowledge and thank the Department of Chemical and Life Engineering at Virginia Commonwealth University. I would also like to thank Xiaojuan Zhang for her helpful and valuable suggestions throughout the course of this research.

I would like to dedicate this research work to my dad, who made who I am now and I will be always grateful. To my lovely mom who has always encouraged me to pursue my goals, always succeed, and never admit defeat. From them I have learned to be the best that I can be. To my sister Jihane, my brothers Mourad, and Karim, thanks for being a constant source of motivation and encouragement. To Rihab Jalal who has been always there for me and my best friend. Thank you all for being a part of my life.

Table of Contents

List of Tables

Table Page

List of Figures

Figure Page

Abstract

INVESTIGATION OF THE MECHANICAL PROPERTIES OF POLY(ETHYLENE GLYCOL) DIACRYLATE BY NANOINDENTATION USING ATOMIC FORCE MICROSCOPY

By Zouheir Drira, B.S.

A thesis submitted in partial fulfillment of the requirements for the degree of Master of Science at Virginia Commonwealth University.

Virginia Commonwealth University, 2009.

Major Director: Dr. Vamsi K Yadavalli, Assistant Professor, Chemical and Life Science Engineering

Poly (ethylene glycol) (PEG) hydrogel based polymers are among the most widely used synthetic materials for biomedical applications. Because of their biocompatibility, and ease of fabrication, hydrogels are highly suitable for use as constructs to engineer tissues as well as for cell transplantation. A critical parameter of importance for PEG hydrogels is their mechanical properties which are highly dependent on the environmental conditions. Properties of PEG-based hydrogels can be engineered to resemble scaffolds composed of extracellular matrix molecules, which provide structural support, adhesive sites and mechanical as well as biomechanical signals to most cells. The mechanical properties of these synthetic scaffolds can affect the migration, proliferation and differentiation of the cells. Accordingly, it is important to investigate the

mechanical properties of these hydrogels and observe their effect on cell behavior as PEG-based scaffolds for example. In this research, the objective is to measure the mechanical properties such as the elastic modulus *(E_c)* and the stiffness *(S)* of polyethylene glycol diacrylate (PEGDA) hydrogel matrices at the nanoscale. The effect of varying parameters in the fabrication of PEGDA hydrogels including monomer molecular weight, initiator concentration and rates of hydration were investigated via nanoindentation using an atomic force microscope (AFM). Two different silicon nitride based cantilevers were used to study the effect of varying loading rates on the mechanical properties of these materials. Indentation parameters such as loads applied and indent depths were varied for each hydrogel sample. Different models were used to fit the experimental data to obtain the parameters of interest for the material (*E_c and S)*. In particular, the data was best described using the model of Oliver-Pharr to analyze and fit the nanoindentation curves. Scanning electron microscope was used to image and confirm the geometry of the tip before and after the indentation experiments. Under high load and displacement modes, the indentation analysis was relatively easy and the elastic modulus and stiffness values were obtained for all dry PEGDA hydrogel sample. The variation of the initiator concentration has been analyzed as well. The mechanical properties of the hydrogel increase as the amount of the initiator increase in the precursor. The degree of hydration dramatically affects the mechanical behavior of the PEGDA. The presence of water within the hydrogel network weakens the internal as well the external mechanical properties, leading to smaller values of elastic modulus and stiffness compared with the dry condition. The mechanical properties of the indenter (cantilever tips) have significant impact on the results. It is important to study carefully the indenter properties before and after the indentation experiments. Since little work has been done on investigating the mechanical properties of PEGDA hydrogels at the nanoscale via AFM,

the analysis of the mechanical behavior of this type of hydrogel using this strategy is of great importance.

Chapter 1: Hydrogels and their mechanical characteristics

1.1 Introduction to hydrogels

Hydrogels are crosslinked hydrophilic polymers that represent an important class of biomaterials in biotechnology and medicine because of their excellent biocompatibility, minimal tissue damage and inflammatory response [1, 2]. Considered as multifunctional polymers, they are used in a variety of applications including as scaffolds for tissue engineering, vehicles for drug delivery, contact lenses, cosmetic products and biosensing [3-9]. Hydrogels can also swell large quantities of water giving them physical characteristics similar to soft tissues. In addition, they have high permeability for oxygen, nutrients, and other water-soluble metabolites. The use of hydrogels has become widely prevalent in the bioengineering fields because of their viscoelastic characteristics, biocompatibility, ease of fabrication into specific shapes and their ability to allow transfer of gases and nutrients [10].

Over the past three decades, a number of hydrogels differing in structure, composition, and properties have been developed [1]. They can be made from chains of natural polymers such as collagen or silk or from synthetic polymers such as poly (ethylene glycol), poly (vinyl alcohol) (PVA) or poly (ethylene oxide). There are three types of synthetic hydrogels that have shown satisfactory results when used in medical applications and specifically in tissue engineering. Double network hydrogels have shown high mechanical properties but no biocompatibility and small biodegradation once placed *in vivo*. Photopolymerizable hydrogels have shown interesting biocompatibility and biodegradability, in addition to their ease of fabrication and the ability to be applied in situ, but mechanically weak. Recently, nanocomposite hydrogels have been developed

to target bioengineering applications. Table 1 presents the different types of hydrogel and their method of preparation.

Classification	*Method of preparation examples*		
Physical HGs	***Hydrogen bond interaction***	***Hydrophobic interactions***	***Ionic interaction***
	PVA, PVA/PEO blends PVA/ poly-gamma-glutamic acid blends PVA/PEO-PPO-PEO blends PVA/poly (vinyl pyrrolidone0 (PVP) blends polyacrylamide/polyarcylic acid blends gelatin, Percec oligodexyribonucleotides-graft-poly	poly (N-isopropylacrylamide) hydroxylpropylmethyl cellulose PE0-b-PPO-b-PEO PPO-b-PPO, PLGA-PEG-PLGA PEG-PLGA-PEG	Alginate chitosa hyaluronan
	Protein interactions	***Chemical reaction***	
	Synthetic polymer-graft-proteins synthetic polymers-graft-coiled coils, biotin-avidin cross-linked networks antigen-antibody cros-linked networks	Reactions used to crosslink natural or synthetic polymers, polymer networks	
Chemical HGs	***Polymerization***	***Chemical reaction***	
	Vinyl monomers	Reactions used to crosslink natural or synthetic polymers, polymer networks	

Table 1 Different method of preparation for both physical and chemical hydrogels (adapted from *Journal of Pharmaceutical Sciences, 96 9 2007*)

Many natural and synthetic polymer hydrogels are used in constructing engineered tissues, drug delivery systems, actuators, sensors, conducting polymers, cosmetics and food applications [11, 12]. These hydrogels include agarose, alginate, chitosan, collagen, fibrin and hyaluronic acid as natural polymers [13], and, poly (ethylene glycol) (PEG), poly(acrylic acid) (PAA), poly(vinyl alcohol) (PVA) and poly (ethylene oxide) (PEO) as synthetic polymer [14]. By developing stronger and more versatile hydrogel networks (double networks, nanocomposite hydrogels) we can expect a much wider range of new applications, but at the same time more design models (theory) and techniques are required to measure and analyze their mechanical properties [11, 15].

1.2 Mechanical characteristics

Hydrogels are 3-dimensional polymeric networks of hydrophilic polymers that are insoluble in water, where they swell to an equilibrium volume but retain their shapes [16]. They have interstitial spaces that can hold as much as 90-99% w/w water [8]. The presence of residues such as hydroxyl (–OH), carboxylic (–COOH), amidic (–CONH–), primary amide ($–CONH_2$) and sulfonic acid ($–SO_3H$) groups on the backbone or as lateral chains result in their high hydrophilicity [16]. In addition to their degree of flexibility analogous to natural tissue, hydrogels have two primary mechanical properties that account for the elasticity and viscoelasticity of the material– once hydrogels are swollen, they exhibit elastic criteria including high extensibility generated by low mechanical stress, complete recovery after deformation, and high extensibility and recovery that are driven by entropic rather than enthalpic changes [17]. At low temperatures, these hydrogels behave viscoelastically and the time dependence of the applied load (stress or strain) is as significant as the magnitude in predicting the material's mechanical response [18]. Unlike normal rubber-like materials which depend on the light crosslinking and the large free volume, the mechanical behavior of hydrogels primarily depends on the architecture of the polymer network. Therefore analyzing the polymer structure, determining the effective molecular weights between cross-links, providing clear information about the number of elastically active chains and cyclization versus crosslinking tendencies within the polymer network, will help in understanding the mechanical behavior of hydrogel [18]. This in turn, will help in the design of hydrogels for novel structural applications.

1.3 Applications and modification of the mechanical properties of hydrogels

Engineering the mechanical properties of hydrogel has been of great interest, especially in tissue engineering applications [3, 10]. Early methods of biomaterials synthesis, including crosslinking and copolymerization of reactive polymer precursors and polymer-polymer reaction have limited the control of the hydrogel structure due to side reactions, unreacted pendant groups, and entanglements [14]. This has led to hydrogels generally having slow or delayed response times to external stimuli (such as temperature, solvent polarity or light) [19]. Several approaches have been examined in order to minimize these limitations. Hydrogels elasticity can be modified by changing the crosslinking densities and other properties such as swelling/collapse or solution-to-gel transitions [8].

The most common examples where hydrogels are continuously modified and used in mechanical application are related to synthetic connective tissues such as articular cartilage, tendons and ligaments [15, 20]. PVA hydrogels have been investigated and serve as strong candidates for artificial articular cartilage because of their strong mechanical properties [21]. However numerous challenges remain in the development of products that can be applied *in vivo*. Hydrogel based materials require certain amount of strength, stiffness, elasticity and resistance. Consequently, engineering their properties for various applications requires measurement and analysis of the mechanical properties of hydrogels including viscoelasticity, stiffness and tensile strength.

For example, prior attempts using hydrogel-based scaffolds in bone and cartilage produced tissues with significantly inferior mechanical strength than the real tissues [22-24]. To improve the mechanical behavior of hydrogels, many variations of methods of synthesizing hydrogel polymers have been developed. These include sliding crosslinking agents, double

network hydrogels, photopolymerizable hydrogels and nanocomposite hydrogels (i.e. poly(acryl amide) and poly(vinyl alcohol)–silicate nanoparticle) [19, 21, 25-27]. The concept of sliding crosslinking agents has shown exceptional mechanical properties with high degree of swelling as well as a high stretching ratio without fracture [14]. Double network hydrogels in turn, are combinations of two hydrophilic networks, both highly and loosely crosslinked polymers mixed together. An example hydrogel with outstanding mechanical properties is composed of two mechanically weak hydrophilic networks – poly (2-acrylamido-2-methylpropanesulfonic acid) and polyacrylamide. These hydrogels contain about 90% water and possess an elastic modulus of 0.3MPa and fracture stress of 10MPa [14]. Nanocomposite hydrogels are a relatively new type of hydrogels which possess unique physical properties due to the presence of nanoparticles within the crosslinked polymer network. Work by Mu and Zheng [28] crosslinking PNIPAM (Poly(N-isopropylacrylamide)) hydrogels with hydrophobic polyhedral oligomeric silsesquioxane (POSS) exhibited remarkable increase in the temperature swelling/de-swelling kinetics, in addition to the improvement of the mechanical strength of the hydrogels caused by the POSS cross-linkers [28].

Paxton et al. have shown that the addition of hydroxyapatite (HA) to a PEG hydrogel increases its mechanical strength, capacity to bind cells, and the ability to interface with biological materials [29]. All these different types of hydrogels have been applied in several applications and analyzed with advanced techniques from the macro-level to much smaller scales. However, issues associated with biodegradability, biocompatibility and mechanical strength still remain.

1.3.1 PEG hydrogels

One of the most remarkable and widely used hydrogels are poly (ethylene glycol) (PEG) based materials. PEG (Figure 1) is a water soluble and biocompatible polymer that has been used in wide ranging biomedical and biological applications [30-32] due to its hydrophilicity and non-toxicity. It can be used and injected inside the human body which makes it ideal for clinical applications. An important property that this polymer holds its extraordinary resistance to protein adsorption which allows PEG-based hydrogels to act as blank slates for cell adhesion [33]

Poly(ethylene glycol) diacrylate (Figure 2), is a three dimensional polymer network formed by substituting the hydroxyl groups of PEG with acrylate functionalities. Crosslinking the PEG polymer has been achieved by different methods [34, 35] - the most common and efficient method being photopolymerization.

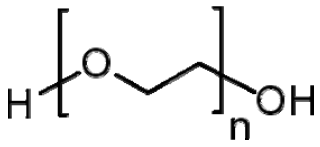

Figure 1 Structure of Poly(ethylene glycol) monomer

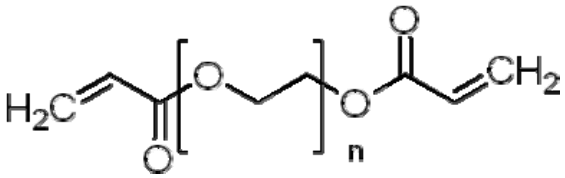

Figure 2 Structure of Poly(ethylene glycol) diacrylate monomer

Photopolymerization has several advantages over conventional polymerization techniques, including spatial and temporal control, fast curing rates and most importantly polymerization *in situ* from aqueous precursors in a minimally invasive manner [1].

Photopolymerization can be used to form crosslinked hydrogel networks by taking advantage of the pendant acrylate groups at the end of each PEGDA molecule. Acrylate monomers are widely used and among the most reactive systems that can be crosslinked by a free radical mechanism (Figure 3). The physical properties of these hydrogels vary not only with the initiator concentration, but also with the molecular weight of the monomer and its concentration. The initiator concentration can affect the degree of crosslinking of the polymeric chains and thereby alter its physical and chemical properties. The ability of these highly tunable hydrogels to provide a wide range of applications is due to specific mechanical properties and responsive behavior to external factors and environmental conditions.

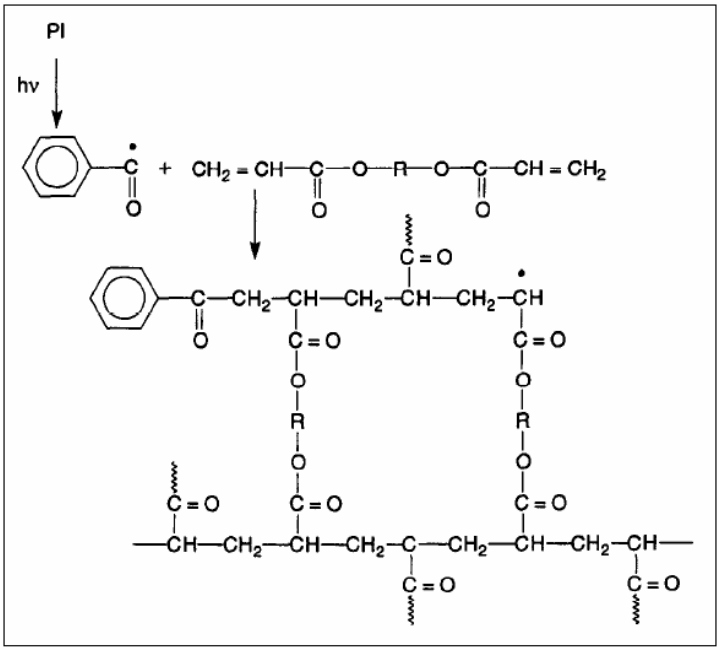

Figure 3 Schematic of a photoinitiated crosslinking polymerization of a diacrylate monomer in the presence a photocleavable aromatic ketone (photoinitiator such as Darocur 1173) [36]

Chapter 2: Measurement of mechanical behavior of hydrogels: bulk level to the nanoscale

Quantitative analysis and study of the mechanical behavior of materials at the nanoscale has become increasingly practicable with the development of micromechanical contact models [37]. A number of different techniques have been developed that are capable of such measurements from the bulk scale to the micro/nano-scale.

2.1 Bulk methods

There are several methods used to define mechanical properties of any polymeric materials including hydrogels at the macroscale. The traditional tensile test consists of taking the sample material and stretching it using, for instance, an *Instron* (Instron, Norwood, MA) tensile machine [38]. This instrument clamps each end of the sample, stretches it, and measures the force (F) exerted. Such instruments can provide important information about such materials including percent-elongation, elasticity, elastic hysteresis and the modulus which measures the resistance of the material to deformation. Several commercial companies develop instruments for the measurement of such parameters including *Instron (Norwood, MA)*, *Sunteccorp (Novi, MI)*, *Knight Mechanical Testing (KMT) (Fort Wayne, IN)*. The macroscale studies of the mechanical properties of polymers are well monitored, but further developments are needed for applications involving hydrogels, particularly for biomedical applications.

In addition to tensile testing of materials, another strategy to determine mechanical properties is to deform the material of interest using an indenter. This consists of applying a normal force to the material of interest using a tip and measuring the changes in morphology of the surface and/or the motion of the tip. The indenter is driven by applying a load at a single

point to a known displacement depth or at a known load. The indentation process generates a load-depth curve (Figure 4) that is used to measure the mechanical properties of the material such as hardness and elastic modulus. Indenter geometry is important for this technique and plays a big role in measuring the mechanical properties as well. By applying the indenter to sample material for a fixed amount of time and at constant displacement, stress relaxation data can be obtained [24]. Indentation can be performed both at the macro as well as the nanoscale depending on the order of the forces applied and the displacements achieved. Because of the ability to perform indentation in real times and measure localized mechanical properties on the surface of the material of interest, indentation has become one of the most common techniques used to characterize the mechanical behavior of wide range of materials including metals, tissues, biomaterials as well as soft polymeric material (hydrogels).

With this technology, the transition to micro-level has been relatively fast. Sophisticated instruments have been developed at this length scale including automatic microhardness indenter (Fischerscope H100C, Fischer, Germany) where both macro-mechanical (strength and modulus of elasticity) and micro-mechanical (hardness, modulus of elasticity and creep) properties can be determined [38]. Lin et al. have shown that once indentation is applied to soft materials including hydrogels at much smaller scale (micro to submicron), they undergo purely elastic deformation even at large indentation depths and the physics of this process becomes more complex and hard to analyze [56]. One example of an instrument that can perform indentation at the microscale is optical-coherence-tomography (OCT) based spherical microindentation technique [56]. This complexity consists of many manifestations and effects including the tip-sample interactions (adhesion), applied forces (too small with soft material: hydrogels) which makes it hard to

identify the point of contact and finally the unclear linearity transition (linear to non-linear) of the stress–strain behavior [56].

Novel multi-function tribological probe microscopes (TPM) can measure several properties - area mappings of topography, friction, Young's modulus and nanohardness [39]. With the continuous increase in the development of nanotechnology and nanoscience in general, new concepts at the molecular and atomic level have been derived, leading to the need for sophisticated and versatile tools and procedures to investigate the mechanical properties and behaviors of the biomaterials as well as the synthetic material developed.

2.2 Mechanical properties of polymers at the nanoscale

Polymers consist of a wide range of properties that are strongly dependent upon their chemistry, molecular architecture, and processing history [40]. At the nanoscale, these properties become more significant, leading to a variety of complex analyses different from the bulk scale. The intermolecular forces are higher causing distinctive methods of control, introduction to statistical thermodynamics and understanding the quantum mechanics involved. On the other hand the structure analyzed at the molecular level is totally different from the macro-level (bulk). Therefore, we have to consider the processing and examine the different reactions involved to form the polymer used. All of the mentioned above come in play when using nanoindentation methods that account for the effects of viscoelasticity where behavior of the investigated polymers is obtained by analyzing the time-dependent deformation characteristics, adhesion forces interpreted in the context of differences in the surface chemistry and variations in the local microstructure [41], in addition to cantilever selection, hydration, and surface preparation considerations [42].

While most mechanical measurements have been made at the macro and micro level [18, 43] an increasing area of application of hydrogels is in the engineering of surfaces that are capable of modifying cellular function and morphology [20, 44]. Protein-protein interactions which guide cellular behavior appear to be guided by the nanoscale architecture of the surface they are tethered on. In particular, recent advances have shown that the behavior and lineage of cells is dictated by the stiffness and mechanical nature of the surfaces they are attached to [45-47]. Since the control of surface properties is becoming significantly important in biology, biomaterials and tissue engineering, the need to characterize the mechanical properties of these materials at the nanoscale is of outstanding interest.

For instance, with the development of new hydrogels, optimization would be advanced by "high-throughput" methods that enable rapid, automated measurements of the elastic modulus. Again, traditional tensile and compression tests are inadequate since they are based on a slow "one at a time" measurement paradigm. In these respects, local probe techniques, in particular nanoindentation, are attractive [48]. The methods mentioned above vary with the ability of measuring the mechanical properties of materials at smaller scales to the possibility of obtaining the elastic properties and hardness of very soft and thin polymer samples, since the displacement and the load of the indenter can be monitored with high precision and accuracy [49, 50]. One of these relatively new techniques of characterizing polymers at the nanoscale is called nanoindentation.

2.3 Nanoindentation

In the last decades, the extension of indentation experimentation from the macro to the nanometer range corresponded with the development of instruments capable of measuring load and displacement throughout a nanoindentation test [51]. Nanoindentation has been widely used to measure and analyze the material properties on the local scale of huge list of different materials including tissues and biomaterial such as bone and cartilage, biomolecules such as DNA-protein, cell membranes, composite materials and polymers such as hydrogel based materials [41, 52-56].

The ability to investigate small loads on the order of several nanonewtons and displacement of about 1 nm has greatly encouraged the study of nanomechanical properties of materials including elastic modulus, hardness and stiffness (which can be measured from a load-displacement curve).

During a typical nanoindentation test, force and displacement are recorded as a three-dimensional indenter tip is pressed into the test material's surface with a prescribed loading and unloading profile. The response of interest is where the force F and penetration depth h are varied and measured by analyzing the loading – unloading curves generated (Figure 4) [57].

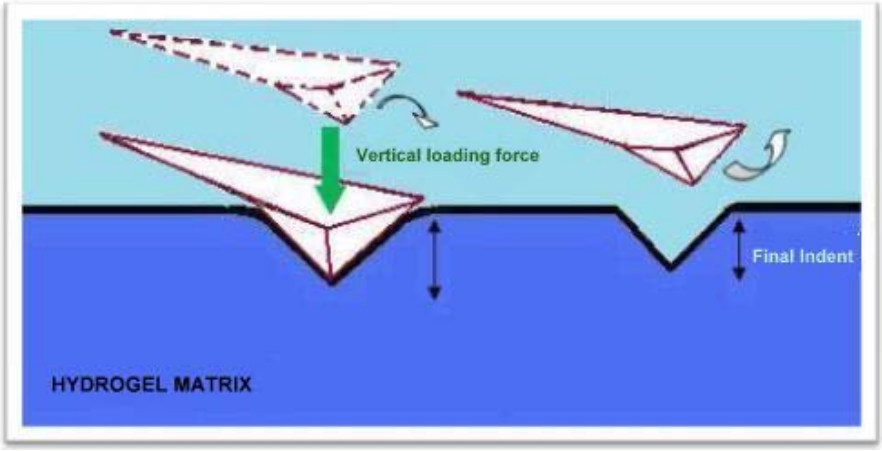

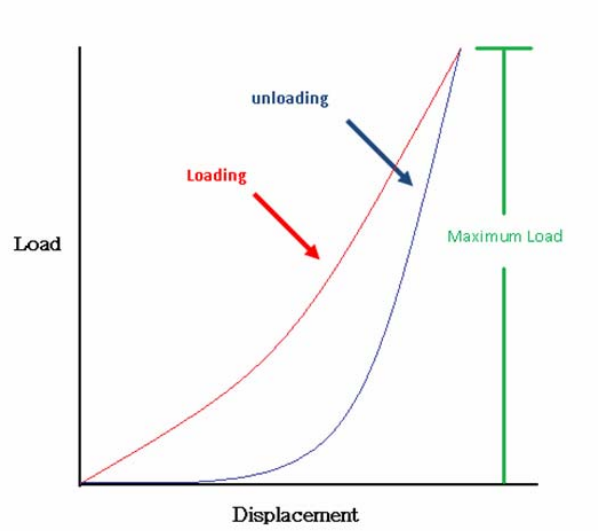

Figure 4 Schematic representation of indentation experiment associated with loading and unloading curves

Instruments for nanoindentation require several essential components [58]. These include a loading unit (indenter), sensors to record the displacement of the indenter (usually attached to a controlled assembly), a two or three –coordinate stage for the sample displacement in x, y or z, a high resolution optical microscope to observe and choose the point of indentation and a computer with a software package to control the operations of the instrument including collection, analysis, and storage of the data [3]. Different indenter shapes have been used including spheres, cones

and pyramids. The most common indenter used in nanoindentation experiments is the Berkovich trihedral pyramidal indenter (Figure 5) [59]

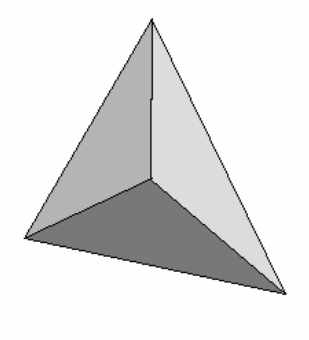

Figure 5 Berkovich trihedral pyramidal indenter

Nanoindentation offers the ability to conduct direct mechanical tests at very light loads (on the order of a few nanonewtons) and small displacements (on the order of a few nanometers). In addition, it also provides the capability to separate the mechanical behavior of different material constituents, using depth sensing to detect phase transformation and investigate the plasticization of polymers [41]. Once soft polymeric surfaces such as hydrogels are indented, the complex viscoelastic –elastic responses induced result in several challenges. This is typical for polymers having strain and strain-rate dependent properties. Therefore, the visco-elastic response of these polymeric materials affects the measurement of the mechanical properties such as elastic modulus and hardness which are a function of the surface contact-indenter geometry, depth as well as the loading rate [60]. Various theoretical and empirical models have been developed to analyze the force-displacement curves generated to account for some of these parameters. These will be discussed in the next chapter.

Regardless of these challenges that can affect the accuracy of the result, nanoindentation remains one of the most powerful techniques used to study the mechanical properties of hydrogels [61] .

There are many high precision indentation instruments that are used to determine the mechanical characterization of soft or hard materials. For instance, the *CSM Indentation Tester* (*CSM Instruments Inc. Needham, MA)* is used to analyze hardness and elastic modulus as well as for characterizing coating adhesion, fracture and deformation at the nanoscale. The *CSM Tribometer* (*CSM Instruments Inc. Needham, MA)* can be used at different length scales (micro and nano) and has the ability to perform nanoindentation under extreme conditions such as high vacuum as well as high temperature environments. Another widely used instrument is the *Hysitron UBi1 Nanoindenter (Hysitron Inc., Minneapolis, MN)*. The UBi1 is a versatile tool for *in-situ* imaging with nanoindentation and nanomechanical property measurement capabilities and can be used on a variety of materials including biological polymers, metals and thin films. It must be noted that most of the indentation experiments performed by the *Hysitron* instruments are destructive and can damage the sample. Mechanical properties are calculated by measuring the dimensions of the material after the destructive load is applied. In addition to these specialized nanoindentation instruments, a tool that is finding increasing application in nanomechanical characterization is the atomic force microscope (AFM). While primarily used for imaging and force spectroscopy, it has been adapted for such measurements as discussed in the next chapter.

Chapter 3: Nanoindentation of hydrogels using atomic force microscopy

3.1 Atomic force microscopy

Since the invention of the atomic force microscope (AFM) primarily as an imaging tool in the late 1980s [62], instrumental developments have vastly expanded the repertoire of novel applications of this instrument over the last two decades to include force spectroscopy, nanolithography and nanoindentation [63, 64]. Today, the AFM has become one of the most versatile tools to study local surface interactions by means of force-distance curves as well as providing an imaging platform to obtain surface morphology [63, 65, 66].

The introduction of AFM-based depth sensing nanoindentation has allowed the analysis of local hardness and elastic properties at the submicron dimensions. One of the earliest works to use AFM to measure mechanical properties was performed by Domke et al. [67] who studied the elastic response of thin soft films of gelatin. Once nanoindentation is applied to soft materials that undergo purely elastic deformation even at large indentation depths, the physics of the process are inherently more complex [67, 68]. This problem has resulted in the push to develop better models and more appropriate approaches to analyze the data and describe the elastic behavior of soft biomaterials or polymer materials in general. In another joint effort, Ebenstein and his coworkers [42] have demonstrated the development of nanoindentation strategies to analyze soft hydrated materials. This method consisted of developing a sample hydration system, selecting the appropriate cantilever for soft material indentation, identify the substrate to be used for blunt tip alignment, and finally determine an appropriate control material for the development of future indentation protocols [42].

In this research we measure of the mechanical properties of hydrogels using nanoindentation, via AFM. The primary advantage of this technique lies in its lateral spatial resolution which allows local testing of mechanical properties in materials that is not possible using macroscale techniques [69-71]. In addition, the AFM provides a real time investigation of materials under different environmental conditions such as in hydrated and dry conditions as well as an analysis of the dynamic mechanical properties such as the strain-rate sensitivity of the material strength [72]. Finally, the application of low loads and/or displacements allows us to interrogate the material of interest in a non-destructive fashion.

3.2 Force-distance curves using AFM

Nanomechanical properties of the polymer are measured by generating a force-distance curve using an AFM cantilever on a sample surface. A force-distance curve is a plot of tip-sample interaction forces vs. tip-sample distance. To obtain a force-distance plot, two simultaneous events are measured- the movement of the AFM cantilevers towards and away from the sample to obtain the cantilever deflection ΔZ_c. The tip sample force is described by Hooke's law (Equation (1)):

$$F = -k_c \Delta Z_c \tag{1}$$

Where k_c denotes the spring constant of the cantilever.

These curves can reveal information about interactions between molecules that are attached to the surface and/or the cantilever (reference). For nanoindentation experiments, specifically, the cantilever is held at the surface and a constant load or displacement is applied.

The distance between the sample surface and the cantilever rest position Z, the tip-sample separation distance D, the cantilever deflection ΔZ_c and the sample deformation ΔZ_s [73] (See Figure 6) are related as:

$$D = Z - (\Delta Z_c + \Delta Z_s) \tag{2}$$

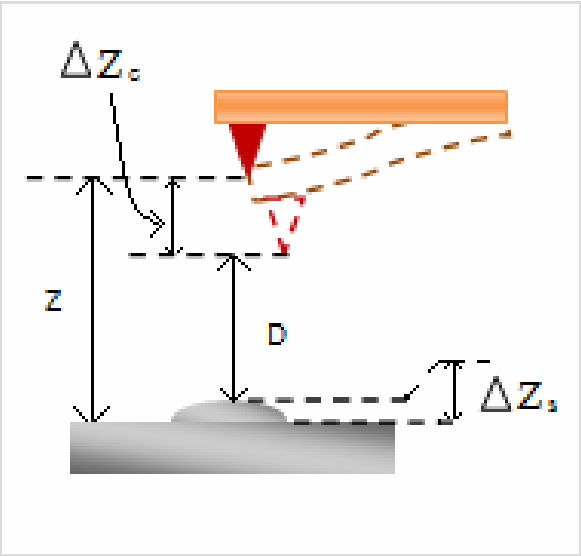

Figure 6 Schematic of the tip-sample system: Both Z and D distances differ due the cantilever deflection ΔZ_c and the sample deformation ΔZ_s

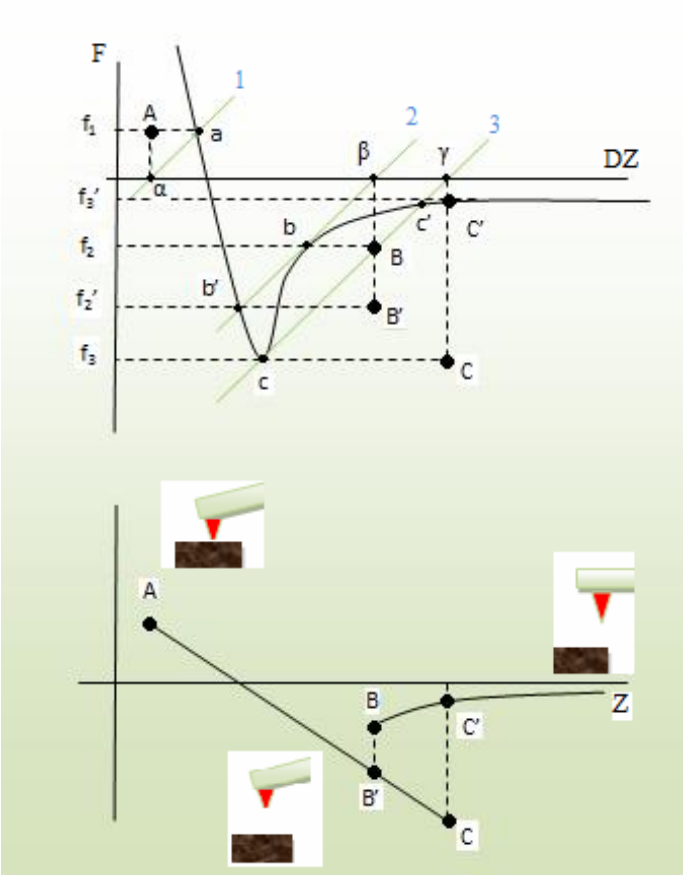

Figure 7 Schematic of a typical force-distance curve obtained via AFM. The first graph (top) represents the interaction force and the elastic force of the cantilever (lines 1, 2 and 3). In the second graph (below), each distance corresponds to a cantilever bending until the elastic force equals the tip-sample interaction force and the system is in equilibrium, (f_1, f_2, f_3 are given by a, b and c between lines 1, 2 and 3). The points A, B, B′, C, C′ in the lower graph correspond to a, b, b′, c, c′ in the upper graph respectively

Figure 7 shows a typical force-displacement diagram as an AFM cantilever approaches and retracts from the surface. In nanoindentation experiments, a constant load or constant displacement is applied to the cantilever at position A resulting in a indentation curve as shown

in Figure 4. The indentation curve reveals two regimes – the loading and unloading of the cantilever as it performs a nanoindentation on the material of interest.

Several theories have been developed to describe the elastic deformation of the sample and the indentation curve generated. The most well-known and applied theory in analyzing the mechanical properties of materials is the Hertz theory. An important approximation in this model is the absence of adhesion or surface forces. Therefore, while using AFM, the Hertz model only applies under high loads and low surface forces [74, 75]. A better approximation is obtained using the Oliver-Pharr model that is described below.

Horkay et al. focused on the theories and analytical models used in measuring the elastic properties of soft materials by conventional nanoindentation [68]. They offer a good interpretation of the Hertz contact mechanics theory which plays a big role in the nanoindentation field and tip–sample adhesive forces/repulsion. Recently, Harmon et al. have used AFM to study the mechanical properties of photo-cross-linked, temperature-responsive hydrogel layers in water [76]. They demonstrated that the elastic modulus differs as a function of the polymer volume fraction, in addition to the investigation on the effect of the cross-linking, density and degree of ionization on the modulus. They used Hertz model that predicts the indentation of a cone or sphere on an elastic sample, and the loading force (F) is a function of the indentation (δ) (Equation (3) and (4) [73]).

$$F_{cone} = \frac{\pi}{2}\frac{E}{(1-\nu^2)}\tan(\alpha)\delta^2 \tag{3}$$

$$F_{sphere} = \frac{4}{3}\frac{E}{(1-\nu^2)}\sqrt{R}\delta^{\frac{3}{2}} \tag{4}$$

where E is the elastic modulus, ν is the Poisson ratio of the soft material, δ is the indentation, α is the opening angle of the cone, and R is the radius of the sphere (Figure 8) .

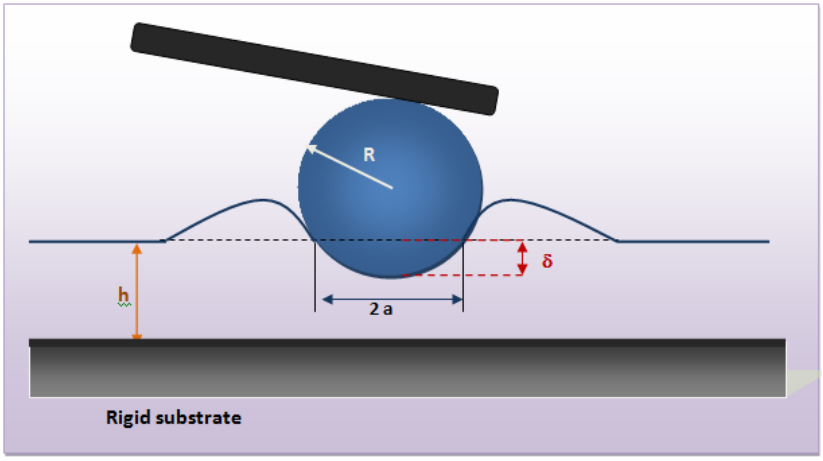

Figure 8 Spherical indenter indenting a soft polymer

The elastic modulus can be calculated from the slope of linear fits to the stress-strain curves [76]. Next, they provided a comparison of these results to rubber elasticity theory for a swollen network in order to study the hydrogel morphology. Through this AFM investigation of a photo-crosslinked type of hydrogel, interesting results showed the behavior of gels under different conditions such as temperature, swelling degree and composition. The elastic modulus values range from 4.5-29 kPa (swollen at 15ºC), and from 470-1300 kPa (collapsed at 42ºC) [76]. This study provided a basis for the development of experimental strategies to obtain results on different characteristics of hydrogels under various conditions (temperatures, compositions, degree of swelling). It also established the application of the AFM as a tool to directly observe the degree of swelling with imaging and simultaneously measure the temperature-dependent elastic modulus using force-distance curves.

3.2.1 Oliver- Pharr stiffness and elastic modulus calculation

It has been shown that nanoindentation can discriminate between similar, low-modulus, hydrated samples [61]. A model that works well for such low-modulus (softer) materials is the theory proposed by Oliver and Pharr [77, 78]. Here it is assumed that during the unloading of the cantilever from the surface, only the elastic displacement is recovered. They estimated the gel elastic modulus using this assumption [78]. The stiffness is calculated by measuring the slope of the upper portion of the unloading curve and is defined as the measure of the resistance of an elastic body to the deformation under an applied load (Equation (6)) [71]. Figure 9 shows the schematic of an indenter as it applies a normal load to a surface.

The unloading curve is usually fit by a power law relation:

$$P = \alpha(h - h_f)^m \tag{5}$$

where α and m are power law fitting constants that depend on the indenter geometry (for example, m ≈ 1 for a flat punch). The stiffness S is given by:

$$S = \frac{dP}{dh} \tag{6}$$

Where dP is the load difference and dh is the displacement difference. For example, using a flat punch indenter, the contact depth is calculated by:

$$h_c = h_{\max} - h_s = h_{\max} - \frac{P_{\max}}{S} \tag{7}$$

where h_{max} and P_{max} are the maximum displacement and maximum load, respectively [71].

The reduced elastic modulus can then be calculated using both the unloading stiffness and the contact area as given by:

$$E_r = \frac{\sqrt{\pi}}{2}\frac{S}{\sqrt{A}} \tag{8}$$

where E_r is the reduced modulus and A is the contact area [71].

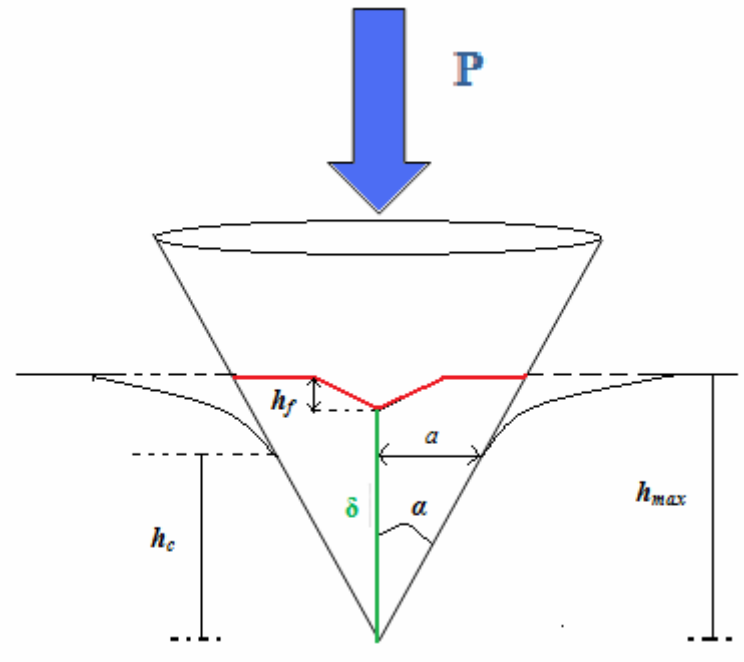

Figure 9 Conical shape tips indenting a soft polymer surface

Notice that both indenter and the hydrogel sample undergo elastic deformation. Therefore, this may affect the reduced modulus calculation, even though the indenter deformation is negligible compared with that of the polymer gel. Equation [73] shows the calculation of the reduced modulus, which is the elastic modulus of the hydrogel sample.

$$\frac{1}{E_r} = \frac{(1-\nu_s)}{E_s} + \frac{(1-\nu_i)}{E_s} \tag{9}$$

Where, v_s and v_i are the Poison's ratio for the sample and the indenter respectively and E_s and E_i are the reduced modulus of the sample and the indenter respectively.

3.3 Elasticity and viscoelasticity

Under small deformations, solids in general store energy and therefore act like a "spring" with an elastic response. Conversely, liquids disperse energy through viscous flow. Complex materials such as hydrogels display viscoelasticity behavior which is a combination of solid and fluid-like response [79]. Recently Yang et al. have used a method of determining the viscoelasticity of hydrogels by measuring the shear modulus as a function of frequency while applying a small amplitude oscillatory shear strain and measuring the resultant shear stress [79]. They also demonstrated that the modulus of the hydrogel (in this case poly (vinyl alcohol)) has significant frequency dependence such that at low frequency the storage modulus dominates the mechanical response while the loss modulus dominates at high frequency [79]. In another study, Tagit et al. [80] used AFM to probe the morphology and the nanomechanical properties of individual PNIPAM (Poly(N-isopropylacrylamide) microgels deposited on surfaces of silicon oxide. The elastic modulus is calculated using the Oliver-Pharr model (Equation (3) and (4)):

$$E = (1-\nu^2)\frac{\sqrt{\pi}}{2}\frac{dP}{dh}\frac{1}{\sqrt{A}} \tag{10}$$

Where ν is the Poisson ratio, *dP/dh* is the slope of the retraction curve, and *A* is the contact area between the tip and the sample [80].

$$A = 3\sqrt{3}h_p^2 \tan^2\alpha \tag{11}$$

where α is the half angle of the indenter and h_p is the effective penetration depth determined from the force–indentation curve [80] .

The value of the elastic modulus obtained for dry PNIPAM spheres in air was reported to be 125.9±0.9 MPa, but when the swollen with water, the modulus of the spheres decreased dramatically to 1.8±0.2 MPa. Above the volume-phase transition temperature in water, the elastic modulus of the spheres increases by an order of magnitude to 12.8±3.6 MPa [80]. This study revealed changes in visco-elasticity of the microgel upon shrinking that cause the cross-linked hydrogel particles to lose water and become stiffer.

Several theoretical methods including the JKR (Johnson–Kendall–Roberts) and DMT (Derjaguin–Muller–Toporov) theory have been proposed to account for parameters such as adhesion between the indenter and the surface [81, 82] However, these methods only work well with rigid materials. In this thesis, the Oliver and Pharr approach has been primarily used as it can be adapted for the indentation of soft materials [18, 68].

3.4 Important considerations

There are several considerations in AFM nanoindentation measurements. These include contact in the "Hertzian" regime and the analytical approaches based on linear elasticity theory such as reference point dependence, methods for non-adhesive and adhesive contact [68]. In addition, hydrogels experience a purely elastic deformation which makes the physical interpretation of the process complicated. Data analysis is difficult due to tip-sample interactions such as adhesion that require the use of more complex models to identify contributions to the interactive forces. In addition, the applied forces for a given indentation depth are really small in soft materials which make the point of contact difficult to identify [68]

Although the elastic deformation range of hydrogels or soft materials in general, is normally larger than hard materials, the transition from linear to nonlinear stress–strain behavior may be vague and unclear. During the AFM experiment, hydrogel samples are subject to water loss, which can significantly influence the mechanical behavior and consequently affect the data collected [18].

Regardless of the goal to improve the analysis of tip-surface interactions and the nonlinearity problem associated with soft material and hydrogel specifically, estimation of the tip geometry and structure remains a real challenge. Many experimental studies have shown reasonable improvement in test structures for SPM (scanning probe microscope) cantilever tip shape deconvolution [83]. While performing indentation experiments, the cross section of the tip and its apex radius of curvature also play a significant role in determining the mechanical properties of the hydrogel material. To better interpret the image data, it is important to determine the tip shape before scanning and check afterwards if it has been changed.

These issues mentioned above can be minimized by the development of new models that extend beyond the Hertzian and linear elastic models to describe the elastic behavior of very thin films. Therefore more work can be done in this area to improve the accuracy for nanoindentation experiments and applications. Future studies will be more focused in the area of nonlinear elastic indentation modeling, which are required to match the fast growth of nanoindentation from polymer science to biology [68].

Chapter 4: Experimental Section

4.1 Materials and methods

Poly (ethylene glycol) diacrylate (100ml), with reported molecular weights equal to 258, 575 and 700 g/mol were purchased from Sigma-Aldrich Co. (St Louis, MO). Photoinitiator Darocur 1173 (Hydroxy-2-methyl-1-phenyl-1-propanone) was obtained from Ciba Specialty Chemicals Corporation (Tarrytown, NY) (see Table 2 for more information). Deionized water (resistivity 18 mΩ.cm) was obtained from a MilliQ water purification system (Millipore Corporation, Danvers MA) and ethanol (200 proof, Absolute, Anhydrous, Shelbyville, KY) were used for experiments. Photopolymerization of the PEG polymer was performed in a UV chamber (Loctite® ZETA® 7401, Loctite Corporation, Rocky Hill, CT, wavelength 360-360nm).

Atomic Force Microscope (AFM) (MFP-3D, Asylum Research, Santa Barbara, CA) was used to obtain images and perform nanoindentation on the PEGDA hydrogel samples. AC 160 TS cantilevers were purchased from Olympus Research (Tokyo, Japan) and PPP-ZEIHR cantilevers were purchased from NANOSENSORS™ (Lady's Island, SC). These two probes were used to image the topography of the PEGDA gel surfaces, as well as to for nanoindentation experiments. To confirm tip morphology, scanning electron microscopy (SEM) images (JEOL JSM-5610LV SEM (Tokyo Japan)) were obtained before and after nanoindentation experiments.

Typical physical properties Photo-Initiators	chemical class	chemical Identity	Appearance	Freezing Point (FP,°C) Melting Point (FP,°C) Boiling point (BP, °C)	Specific Gravity (Water = 1)	UV/VIS Absorption peaks (nm) in methanol
DAROCUR 1173	α-Hydroxyketone	2-Hydroxy-2-methyl-1-phenyl-1-propanone	clear, light yellow liquid	liquid at romm temp. MP 4 °C, BP 80-81 °C	1.1	245, 260, 331

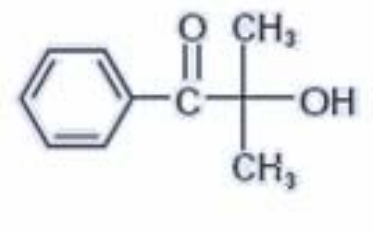

Table 2 Darocur 1173 and its properties (Ciba Specialty Chemicals ,Tarrytown, NY)

4.1.1 Fabrication of PEGDA hydrogels

PEGDA hydrogel samples were prepared by a two step process –

A) 2ml of the PEGDA was mixed with 10 µl of Darocur 1173 (0.5% photoinitiator) in a 15-mL plastic centrifuge tube and vortexed for 20 seconds to obtain a well mixed solution. The same procedure was repeated for the 1.0% and 1.5% initiator which corresponds to 20µl and 30µl of initiator added, respectively.

In order to fabricate uniform slabs of hydrogels, four glass slides and a big size Petri-dish was used (Figure 10). The glass slides were put together to form a slab like mold where the precursor mixture was poured. The Petri-dish was then placed in the UV chamber for polymerization of the monomer. After the UV radiation and photopolymerization, a clear PEGDA hydrogel slab was obtained.

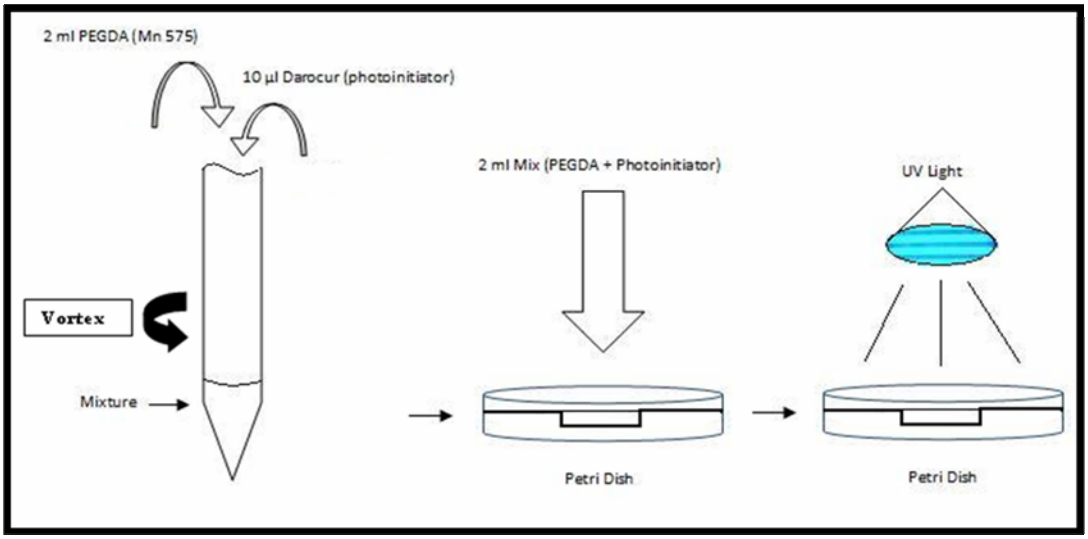

Figure 10 Process of the fabrication of PEGDA hydrogel samples

B) The precursor solution was then exposed to UV radiation (360-370nm, 10 mW/cm^2) (Figure 10) for a controlled amount of time to obtain the polymerized hydrogel. Figure 11 shows the spectral distribution of the lamp used in these experiments.

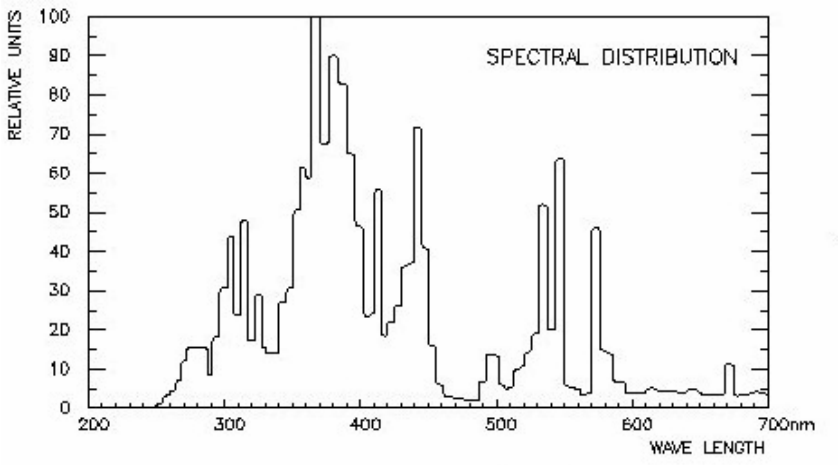

Figure 11 Spectral distribution of the wavelength emitted by the lamp in the UV chamber (Loctite 7401)

Table 3 presents the different conditions for the fabrication of PEGDA hydrogels used in these experiments. The compositions of the initiator and UV radiation time were optimized over several trials to obtain a relatively well shaped and uniform sample with a clear morphology (see Results).The amount of the PEGDA solution was always kept fixed with different amounts of initiator. The optimal time interval for photopolymerization was determined to be in the range of 45-60 seconds.

Trial	PEGDA 575 sol. (ml)	Darocur 1173 sol. (µl)	UV light time (sec)	Drying time/swelling
1	2.5	15	30	overnight oven 50˚C
2	3	15	40	overnight oven 50˚C
3	2	10	120	overnight oven 50˚C
4	2	10	45, 40	At room temperature
5	2	10	45	overnight oven 28˚C
6	2	10	60, 70	overnight oven 28˚C / At room temperature
13	2	15	50,40	At room temperature
14 (2 slides)	2	20	100	At room temperature
16	2	30	40,60	At room temperature

Table 3 Different trials and compositions of the mixtures, UV light timing and the drying conditions adopted in the fabrication of hydrogel films

4.1.2 Hydration condition of the hydrogel samples

Two main conditions of the hydrogel matrix were considered for these experiments - dry and wet. Wet samples were assessed on the basis of the final water content of the material. The different steps taken prior to formation of the final product are presented below.

After the hydrogel sample was photopolymerized, it was washed with water for 8 to 10 minutes and dried. The drying times and methods varied from using a convection oven to drying at room temperature. It was observed that while using the oven, the rate of heating was higher that caused faster drying but resulted in breakage and cracking of the sample. On the other hand, letting the sample to dry in air (room temperature 20-25 ºC) resulted in samples that exhibited a clear surface morphology for nanoindentation experiments. Wet hydrogel samples were prepared by hydrating the sample in water and allowing it to swell to an equilibrated state (usually 24 hours in water). The size and weight of the hydrogel increase confirming the swelling of the sample. Once the sample was removed from the water and weighed, the surface was blown in a gentle stream of air prior to nanoindentation experiments. After the nanoindentation, the sample was weighed again and the percent of water content in the hydrogel was calculated.

Two cases are presented in the analysis 63% and 86% water (Table 4). Since typical applications involving hydrogels, require that the polymer is surrounded by a liquid environment (such as serum or water), it is important to measure the properties of the material in the fully hydrated state. To achieve this, the sample hydrogel was indented directly under water. In this case, the water content of the hydrogel was close to 100%.

4.2 AFM-nanoindentation

The nanoindentation was conducted on PEGDA samples using two different cantilevers AC160 and PPP-ZEIHR with spring constants varying from 30-40 N/m and 15-27 N/m respectively.

The first set of experiments were performed on dry hydrogel samples PEGDA 575, 258 and 700) with different initiator compositions. Only PEGDA 575 with 1% initiator was used for

the wet condition. Table 4 presents the different parameters that were varied through the course of the research, to investigate of the mechanical properties of these poly (ethylene glycol) diacrylate hydrogel materials.

PEGDA (g/mol)	Initiator %			Cantilever		Hydration (wet condition)			Dry
2 ml	0.50% 10µl	1.00% 20µl	1.50% 30µl	AC 160	PPP-ZEIHR	63%	83/%	100%	
258	N/A	✓	N/A	✓	N/A	N/A	N/A	N/A	✓
575	✓	✓	✓	✓	✓	✓	✓	✓	✓
700	N/A	✓	N/A	✓	N/A	N/A	N/A	N/A	✓

Table 4 Summary of the different experiments: Fabrication of the PEGDA hydrogel samples, the cantilever used to perform nanoindentation, and the state of the sample

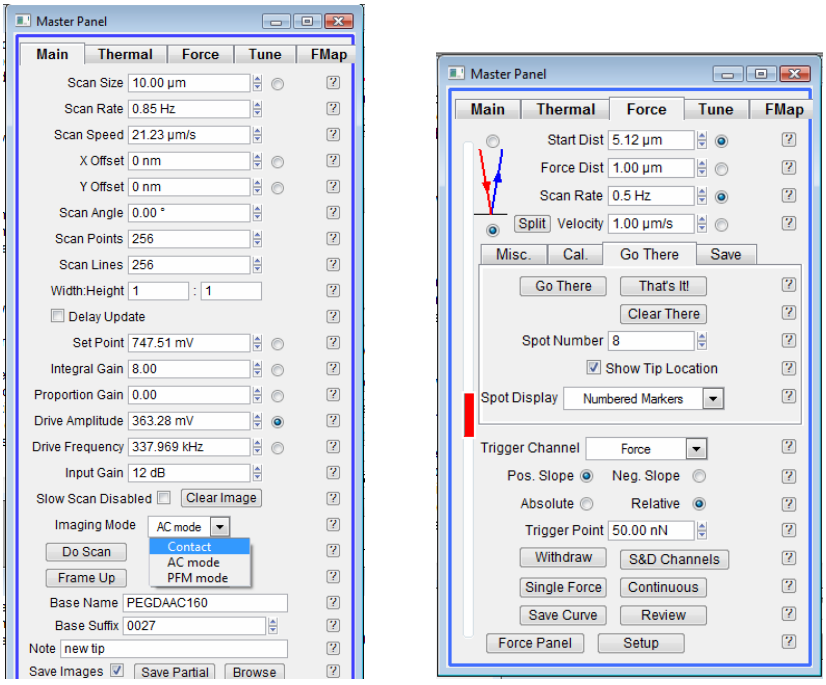

Figure 12 Master Panel and Force Panel in IGOR Pro software

4.2.1 Spring constant calculation

AFM cantilevers can act as micromechanical sensors to determine viscosity, study electrochemistry and detect different gases and vapor [84]. Since all the applications depends on the accurate knowledge of the physical properties of the cantilever, it is very important to measure the spring constant to quantify the forces measured [75].

The spring constant values of the cantilevers were typically provided by the manufacturer, but it is important to measure them before every nanoindentation experiment. To minimize the effect of tip-surface adhesion, for each cantilever used (AC160 TS and PPP-ZEIHR), spring constants were measured on a hard and clean mica surface. The measurement of the spring constant was performed using the thermal fluctuation method [75]. The same procedure was repeated 5 to 6 times on different points of the mica surface. The average of these calculated spring constants was the value used for analysis.

4.2.2 Imaging and nanoindentation experiments

Following the measurement of the spring constant, the first step was to image the surface and determine the topography of the PEGDA hydrogel. The AFM was operated in both non-contact and contact modes (Figure 12). Non-contact (AC) mode was used for imaging the hydrogel surface. It involves an AFM cantilever that is vibrating with a small amplitude oscillation (less than 10 nm) near the surface. The system monitors the vibrational amplitude of the cantilever and keeps it constant with the aid of a feedback system that adjusts the z-piezo in response to topographic information. It was important to use this mode while imaging, because it is capable of measuring the topography with minimal damage to the sample and the cantilever. Non-contact imaging is the best technique for measuring sample topography of soft biomaterial

and polymers in general [85]. Figure 13 shows the non-contact height image of the PEGDA hydrogel surface.

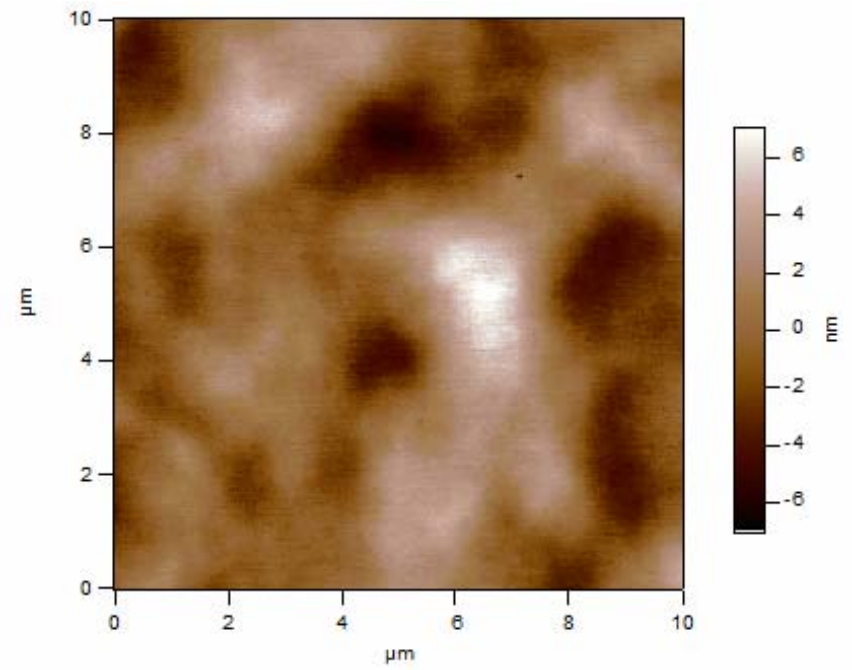

Figure 13 Height image of the PEGDA 575 surface

On the other and hand, contact mode was used for nanoindentation experiments. The AFM cantilever tip was engaged on the surface of the hydrogel. The next step was to select the indenter mode (Figure 14), (two modes were chosen: load or displacement), select a loading rate and a maximum load that could be applied to the surface.

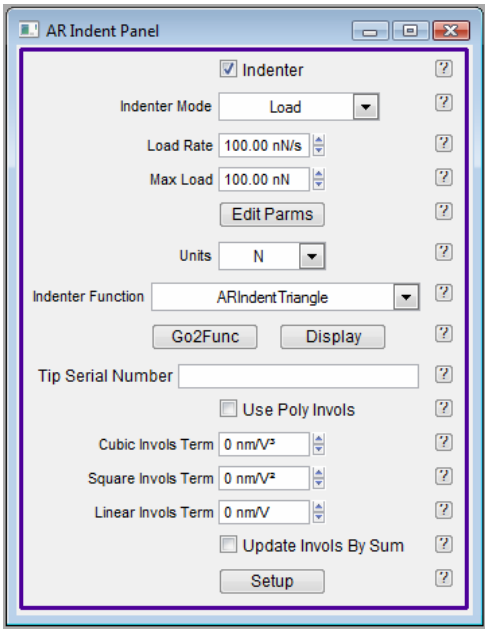

Figure 14 Indenter Panel in IGOR Pro

Indentation experiments were performed under two distinct regimes – constant displacement and constant load. Table 5 shows the load and displacement values that were used for these experiments. For each material, we wished to perform the experiment at two distinct conditions – a high and low load and displacement. The high load was selected to be 150nN and the low load was selected to be 20nN. The high displacement was selected to be 100nm and the low displacement was selected to be 10nm. It is important to mention the choice of these values. Before collecting the data for the analysis of the mechanical properties (elastic modulus and stiffness) of the PEGDA hydrogels, several trials were performed by varying different experimental parameters and conditions in each mode. At these values, especially at high load and displacement, nanoindentation curves with a high signal to noise ratio that could be satisfactorily fit to the theoretical models were obtained. The low load and displacement values were chosen to compare the data collected with the high load and displacement result.

	PEGDA 575 & 700 *(w/t 1% Initiator)*	PEGDA 258
	High Load	
LR (nN/s)	100	50
ML (nN)	150	50
TP (nN)	50	20
	Low Load	
LR (nN/s)	5	5
ML (nN)	20	20
TP (nN)	10	10

	PEGDA 258, 575 & 700 *(w/t 1% Initiator)*
	High Displacement
DR (nm/s)	100
MI (nm)	100
TP(nN)	30
	Low Displacement
DR (nm/s)	10
MI (nm)	10
TP(nN)	5

Table 5 Different modes and values associated with nanoindentation experiments

4.2.3 Data analysis

The nanoindentation curves were analyzed using standard routines in the technical graphing and data analysis software IgorPro (WaveMetrics, Inc., Portland, OR). In order to fit the data, two commonly used models (described in Chapter 3) were used.

4.2.3.1 Models for the determination of mechanical properties from indentation data

The most common model to fit data for indentation has been the Hertz model [76, 86]. In IGOR Pro, routines to fit data using both the Hertz and the Oliver-Pharr models are available and were used to analyze the data. Since the PEGDA hydrogel material is considered a soft material, it was better to use the Oliver-Pharr model over the Hertz model. The Hertz model is usually used to analyze hard surfaces and mostly for experiments that involve a destructive nanoindentation [59]. In this research, our experiments involved the indentation of the surface of the hydrogel with minimal damage and analyzing the purely elastic response of the material.

This information is contained in the unloading part (as the cantilever retracts from the surface) of the nanoindentation force-displacement curve (Figure 15). This allows simultaneous measurement of both the elastic modulus and the stiffness.

Once the nanoindentation experiments were done, the curves were analyzed using either model (Figure 15 and Figure 16). For the Hertz model (Figure 15), the shape of the indenter (cantilever tip) is the most important parameter that needs to be accurately determined for each trial. This poses a big challenge since AFM tip shape deconvolution is typically not accurate enough to obtain a satisfactory fit of the data via this model [87], The nanoindentation curves obtained in these experiments were not well fit using this model, since any geometry could be selected (punch, cone or sphere) to give a fit. On the other hand, the Oliver-Pharr model (Figure 16) was found to be more suitable for the investigation of the mechanical properties of the PEGDA samples. This model still requires the geometry of the tip and especially its contact area, but can be satisfactorily approximated using a standard tetrahedral Berkovich tip. Since both cantilever tips used in these experiments had tetrahedral geometries, the analysis was more accurate using this model.

Finally, the Poisson ratio of both the tip and the sample need to be selected. Throughout this analysis the Poisson's ratio ν_1 of all the PEGDA samples was assumed to be 0.5. This number was estimated from the literature, where soft hydrogel-based polymers were found to have typical values around 0.45-0.5 [71, 88].

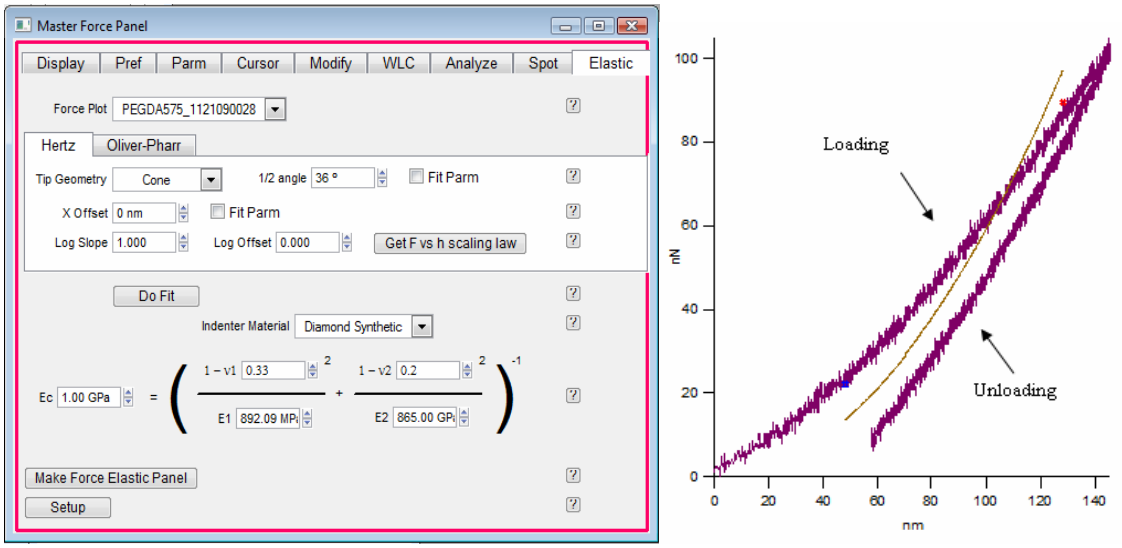

Figure 15 Master Force Panel (IGOR Pro) showing the Hertz Model

The four parameters that are of importance in the Oliver-Pharr model are the Poisson ratio ν_1 (0.5) of the sample, the type of the indenter material, the Poisson's ratio ν_2 of the cantilever material (0.25), and the elastic modulus of the indenter E_2 (290 GPa) for the cantilever. The values used are for a silicon nitride cantilevers (both AC 160 and PPP-ZEIHR). In order to fit the parameters and estimate the elastic modulus of the material, the unloading curve is fit to the Oliver Pharr equation as shown in Figure 16. This results in determination of the reduced elastic modulus E_c and the stiffness S (Figure 16).

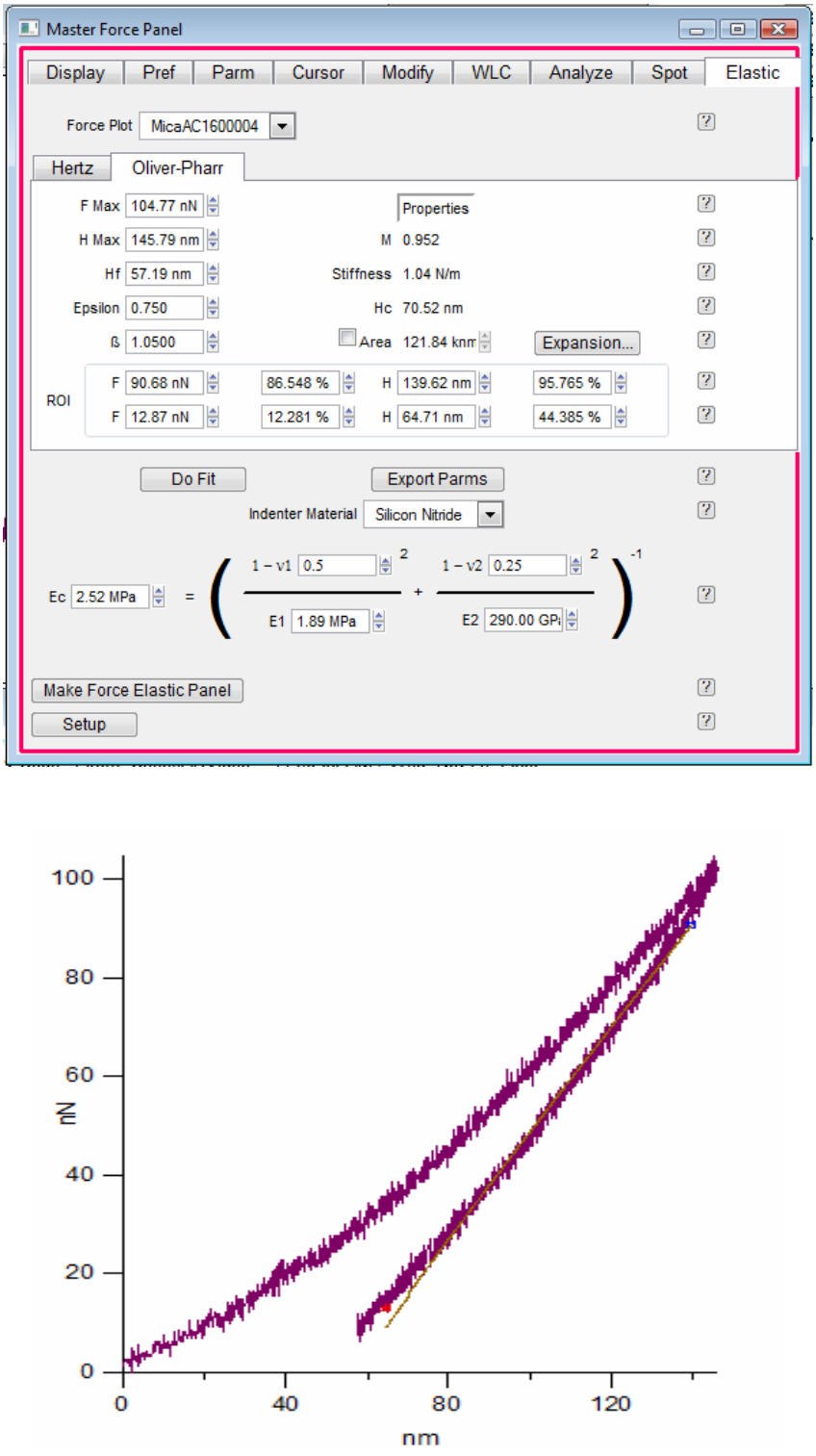

Figure 16 Master Force Panel (IGOR Pro) showing the Oliver-Pharr model

4.3 Scanning Electron Microscopy (SEM) imaging

SEM images of the AC160 cantilever were taken before and after indentation experiments. The cantilever was placed inside the specimen chamber of the JEOL SEM in a position where the tip can be seen (about 40 degrees inclination). Then the vacuum is applied to evacuate the chamber. During this imaging procedure the accelerating voltage setting was initially fixed at 20kV and the Z position at 20 mm. Some images required to change these settings to 15kV in order to get high resolution images. The SEM images were helpful in confirming the tip geometry to calculate the mechanical properties of the PEGDA hydrogel samples. Images taken after nanoindentation allowed us observe any variation in the shape and geometry of the tip as a result of the experiments.

4.4 Preliminary data analysis

The nanoindentation experiments were performed on a 10x10 μm^2 hydrogel surface. For every indentation test, 20 to 25 load depth curves were generated per surface area (20-25 different indentations correspond to 20-25 different location on the surface). Four different areas on each PEGDA hydrogel sample were analyzed. Therefore, about 80 to 100 curves were analyzed per PEGDA slab. The number of samples for each of the PEGDA synthesis conditions is shown in Table 6.

PEGDA (g/mol)	Initiator %			Cantilever		Hydration (wet condition)			Dry
	0.50%	1.00%	1.50%	AC 160	PPP-ZEIHR	60-63%	80-83%	100%	
258	N/A	3	N/A	3	N/A	N/A	N/A	N/A	3
575	4	6	4	14	4	4	4	3	18
700	N/A	6	N/A	6	N/A	N/A	N/A	N/A	6

Table 6 Number of PEGDA slabs used for every condition

The Table below shows an example of 25 indentations performed on one area of the PEGDA 258 and PEGDA 700 surfaces. The average value of the elastic modulus and stiffness were calculated from the analysis of all the curves for each condition. The standard deviation was obtained for each data set as well using Excel (**Table 7**).

	PEGDA 258(Dry Condition) 2ml	
	1 % initiator	
	Tip AC 160 with Sp.cst 37.37 N/m	
	Ec (MPa)	Stiffness (N/m)
	1.39	0.989
	1.32	0.91
	1.29	0.912
	1.35	0.915
	1.3	0.893
	1.38	0.901
	1.34	0.937
	1.32	0.893
	1.35	0.931
	1.28	0.924
	1.25	0.943
	1.3	0.933
	1.45	0.91
	1.4	0.994
	1.36	0.904
	1.34	0.917
	1.35	0.92
	1.31	0.869
	1.34	0.977
	1.34	0.953
	1.28	0.925
	1.32	0.909
	1.3	0.922
	1.31	0.926
	1.34	0.87
Avg 1	*1.33*	*0.92*
STDev 1	0.04	0.03

	PEGDA 700 (Dry Condition) 2ml	
	1 % initiator	
	Tip AC 160 with Sp.cst 37.37 N/m	
	Ec (MPa)	Stiffness (N/m)
	1.91	2.92
	2.33	2.79
	2.63	2.88
	2.67	2.92
	2.64	2.89
	2.63	2.87
	2.64	2.91
	2.72	2.95
	2.77	2.82
	2.58	2.91
	2.77	2.76
	2.67	2.72
	2.65	2.86
	2.77	2.73
	2.7	2.7
	2.62	2.67
	2.74	2.76
	2.74	2.8
	2.62	2.79
	2.72	2.67
	2.72	2.73
	2.82	2.81
	2.77	2.81
	2.86	2.8
	2.71	2.8
Avg 1	*2.66*	*2.81*
STDev 1	0.19	0.08

Table 7 Elastic modulus E_c and stiffness S measurements of both PEGDA 258 and 700

Chapter 5: Results and Discussion

5.1 Results

5.1.1 Fabrication of the PEGDA hydrogel samples

Initially, several trials were performed to optimize the materials used for the indentation experiments. Some combinations of precursor, initiator and UV radiation times resulted in hydrogel samples that were cracked or discolored. Also several samples that were washed with deionized water and kept at room temperature started to show some cracks as well as deformations (Figure 17). In particular, PEGDA hydrogels with a molecular weight of 258 Da resulted in the largest fraction of defective samples.

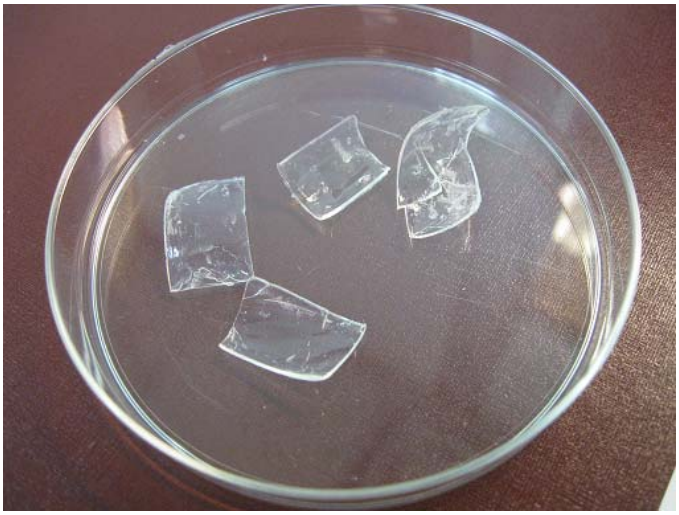

Figure 17 Examples of defective PEGDA samples

On the other hand, PEGDA 575 and 700 hydrogel samples were easy to fabricate and showed a uniform and well shaped slabs. Variables including the amount of initiator added, the UV radiation time and the drying procedure, can all affect the final product for each molecular

weight used. After several trials optimizing these parameters, clear, uniform, and rectangular PEGDA hydrogel samples could be fabricated reproducibly. The final product consists of photopolymerized poly (ethylene glycol) diacrylate hydrogel film of 1mm to 1.5 mm thickness (Figure 18).

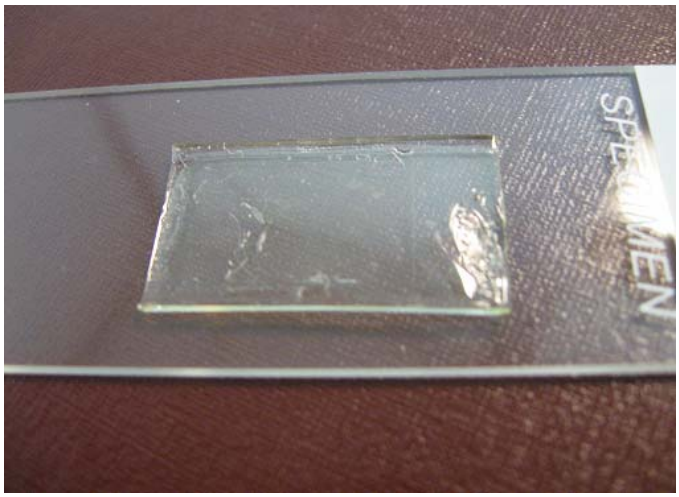

Figure 18 PEGDA 575 Hydrogel sample made on a glass slide and ready for nanoindentation

5.1.2 AFM Imaging

AFM imaging was mostly done in non-contact mode. We used this imaging mode to minimize the chance of contaminating and damaging the cantilever tip as well as the sample surface. On the other hand, contact mode imaging was only used while performing the experiment under water. Figure 19 presents two AFM images taken before (Left) and after (left) nanoindentation. These images were taken using AC160 cantilever under high loads, the small black spots that appeared in the right image (after indentation) in Figure 19, represent the indentation as well as the deformation of the material at these locations. These images reveal the topography of a hydrogel surface, which is a typical polymer surface.

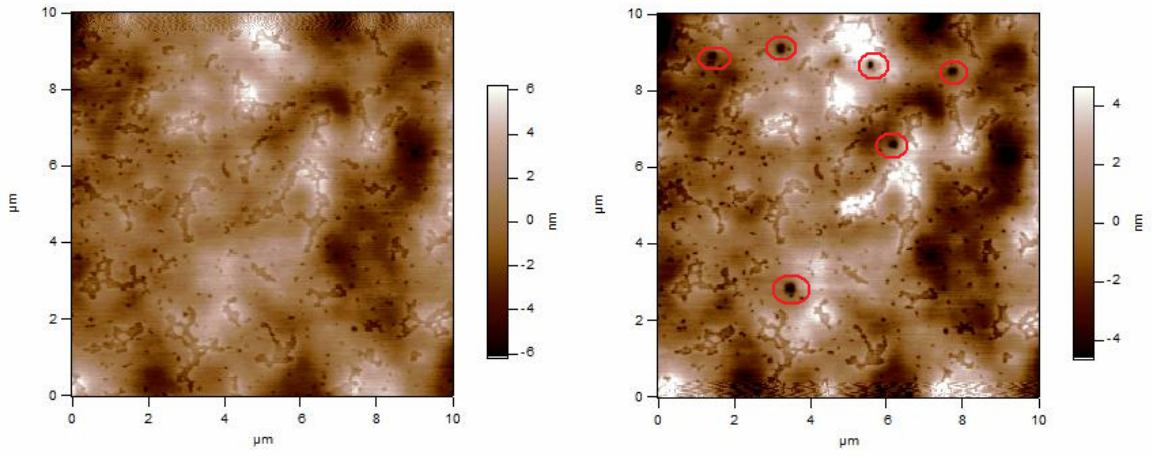

Figure 19 AFM images in non-contact mode of a PEGDA surface before and after the nanoindentation experiment. The figure on the right shows distinct areas of damage (red circles) where the nanoindentation was applied

5.1.3 AFM nanoindentation

The nanoindentation experiments consist of taking force-displacement curves by indenting the surface of the PEGDA hydrogel as described in the previous chapter. Following the imaging of the surface, 25 different points were selected on the surface and the cantilever was moved to each point to obtain under four different indent modes (high and low load, high and low displacement). The AC 160 cantilever (Table 8) was used for all the PEGDA hydrogels, and the PPP-ZEIHR (Table 8) cantilever was used for only PEGDA 575. For example at high load, 25 points at different locations of the hydrogel surface corresponded to 25 different indentations curves. The same procedure was repeated with the four indent modes for PEGDA hydrogels 258, 575 and 700. The results of these experiments are shown in Figure 20, Figure 21 and Figure 22. Each figure shows the overlay of several different indentation curves that were normalized to the same starting point.

In the high load and displacement modes, the curves have a high signal to noise ratio and were easier to fit via the Oliver-Pharr model to determine the elastic modulus and the stiffness. On the other hand, at a low load and especially for the low displacement modes, the curves were generally indistinct and blurry as seen in Figure 21. This high noise is to be expected for such low loads and displacements. Therefore, it was difficult to reliably fit all the data with the Oliver-Pharr model.

AC 160		
Sp.Cst (N/m)	Poisson Ratio	E (Gpa)
[30 - 40]	0.25	250.00

PPP-ZEIHR		
Sp.Cst (N/m)	Poisson Ratio	E (Gpa)
[10 - 60]	0.25	250.00

Table 8 Properties of AC 160 and PPP-ZEIHR cantilever tips

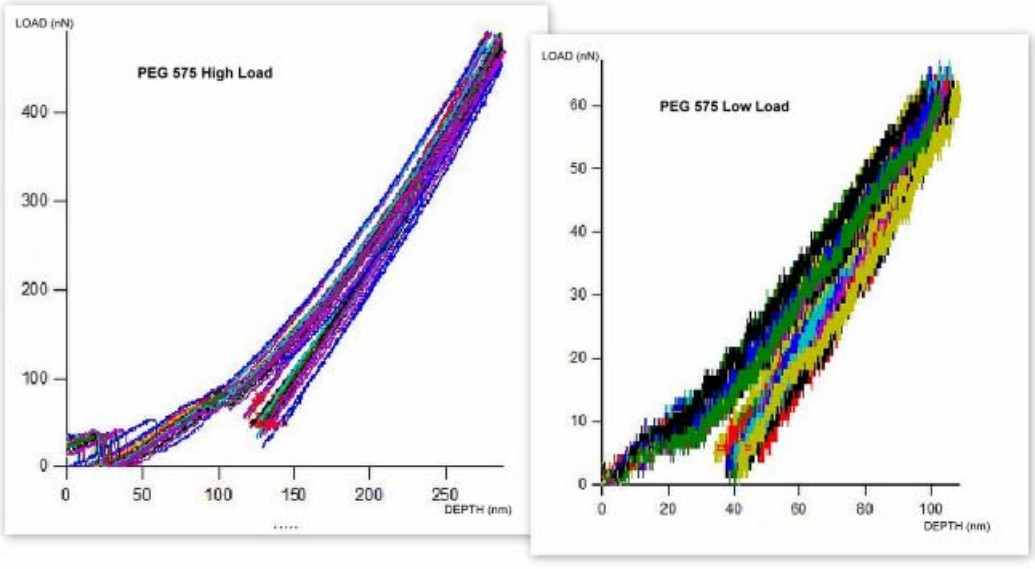

Figure 20 Indentation curves of PEGDA 575 (1% initiator) under High and Low load indent modes using AC 160 cantilever

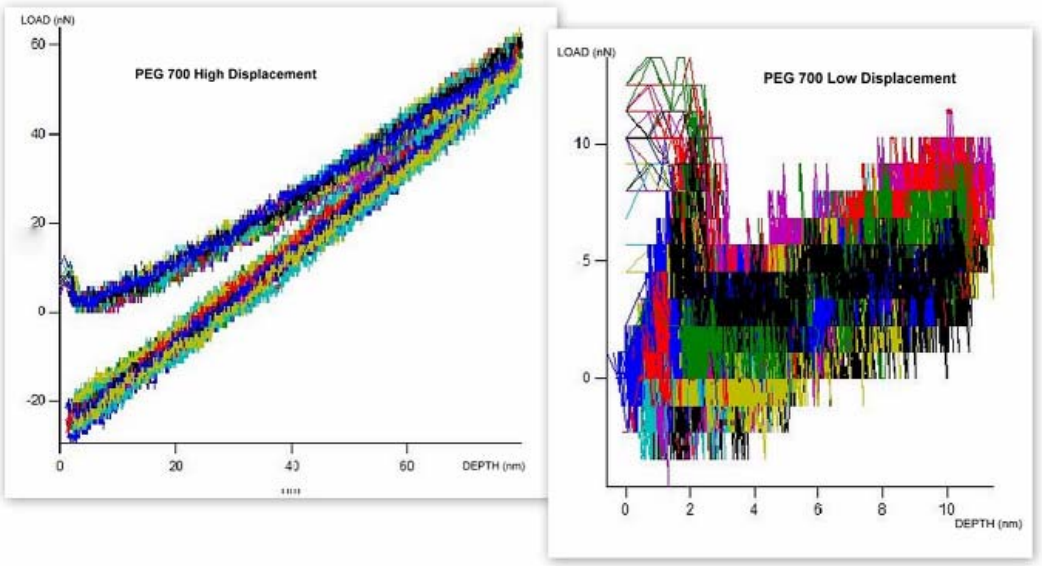

Figure 21 Indentation curves of PEGDA 700 (1% initiator) under High and Low displacement indent modes using AC 160 cantilever

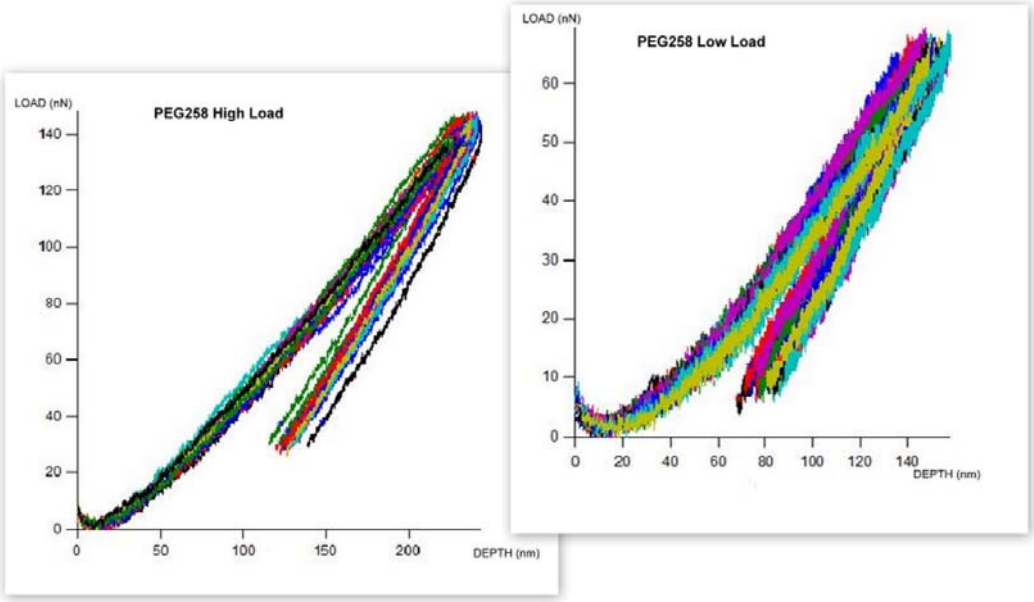

Figure 22 Indentation curves of PEGDA 258 (1% initiator) under High and Low load indent modes using AC 160 cantilever

Under high and low load (150 nN and 20 nN respectively), the depth or displacement cannot be fixed or known before the indentation occurs. This mode only controlled the force pushing the tip into the surface thereby deforming the material. In Figure 20, the maximum depth was around 300 nm into the PEGDA 575 hydrogel sample. Under high and low displacement (100nm and 10 nm) indent modes, the depth is controlled and known. In this mode, the cantilever tip travels a fixed depth into the surface (100nm or 10nm). In Figure 21 the maximum depth was around 100 nm for high load indent mode which corresponded to ~50 nN in load and at a 10 nm for low displacement indent mode, the force corresponded to ~10nN load. All these parameters are important in the measurement and the analysis of the mechanical properties of these sample polymer gels.

In the elastic tab under the master force panel of IGOR Pro, both Hertz and Oliver-Pharr models were included. Since it is a soft material, we used the Oliver-Pharr model to analyze every single curve and obtained the elastic modulus and stiffness data for all three molecular weights of PEG hydrogels. Considering only the unloading part of each curve, both elastic modulus E_c (in circled with blue (Figure 23)) and stiffness S (in circled with red (Figure 23)) of the hydrogel surfaces were calculated. For instance, in the Figures shown, two values corresponding to the elastic modulus and the stiffness of the sample material were obtained for each indentation curve. This data is presented in Table 9.

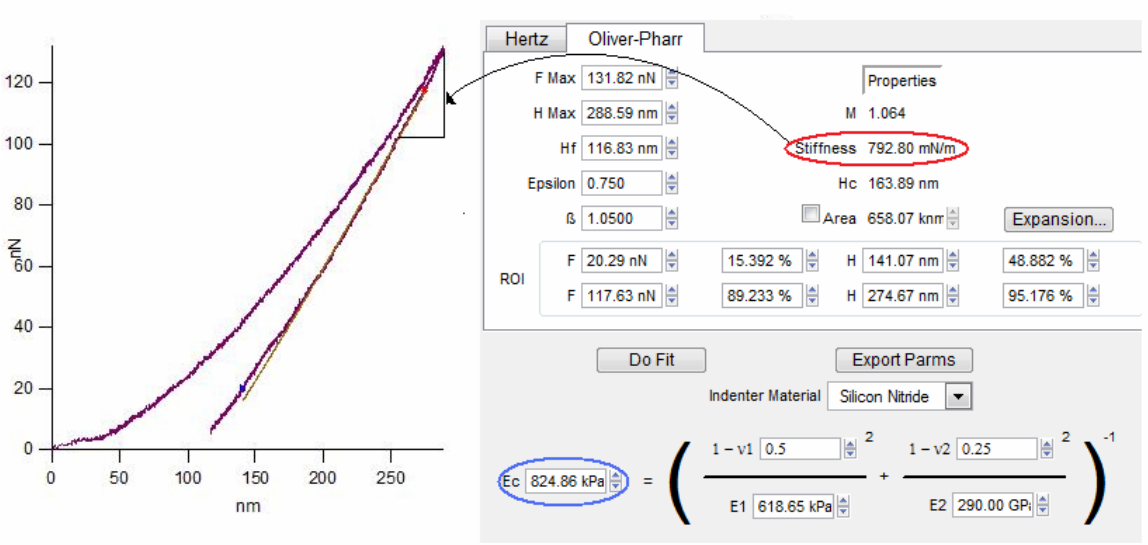

Figure 23 Calculation of the elastic modulus Ec and stiffness S with Oliver-Pharr model

	PEGDA 258		PEGDA 575		PEGDA 700	
	High Load					
	Average	STDev	Average	STDev	Average	STDev
Ec (avg) Mpa	1.33	0.04	3.19	0.38	2.66	0.19
Stiffness (avg) N/m	0.92	0.03	2.83	0.11	2.81	0.08
	Low Load					
	Average	STDev	Average	STDev	Average	STDev
Ec (avg) Mpa	1.58	0.08	3.17	0.15	2.94	0.22
Stiffness (avg) N/m	0.78	0.05	1.00	0.08	1.12	0.09

Table 9 Elastic modulus and stiffness average values of the three PEGDA hydrogels at high and low loads

From Table 9, it can be seen that the elastic modulus of PEGDA 575 polymer gel was the highest at around 3.19±0.38 and 3.17±0.15 MPa, as well as the stiffness with 2.83±0.11 and 1.00±0.08 N/m in the high and low indent modes respectively. On the other hand, PEGDA 258 had the lowest elastic modulus of around 1.33±0.04 and 1.58±0.08 MPa and stiffness with only 0.92±0.03and 0.78±0.05 N/m under high and low loads respectively.

	PEGDA 258		PEGDA 575		PEGDA 700	
	Average	STDev	Average	STDev	Average	STDev
	High Displacement					
Ec (avg) Mpa	3.30	0.11	5.07	0.10	5.23	0.22
Stiffness (avg) N/m	1.33	0.07	1.69	0.06	1.52	0.11
	Low Displacement					
	Average	STDev	Average	STDev	Average	STDev
Ec (avg) Mpa	40.50	13.33	43.45	11.00	43.41	6.00
Stiffness (avg) N/m	2.03	0.99	1.68	0.88	1.48	0.53

Table 10 Elastic modulus and stiffness average values of the three PEGDA hydrogels at high and low displacements

Table 10 presents the experimental data obtained in the high and low displacement modes. It can be seen that the PEGDA 700 hydrogel had the highest elastic modulus value of 5.23±0.22 MPa, whereas PEGDA 575 was slightly lower in value of 5.07±0.1 MPa. The PEGDA 258 had the lowest values of the elastic modulus at 3.30±0.11 MPa. For the stiffness, PEGDA 575 had the highest value of 1.69±0.06 N/m, followed by PEGDA 700 at 1.52±0.11 N/m and finally PEGDA 258 at 1.33±0.07 N/m. Under low displacement indent mode the elastic modulus values were extremely high, but still PEGDA 575 was on top with 43.45±11 MPa, PEGDA 700 with 43.41±6 MPa and then PEGDA 258 with 40.5±13.33 MPa. The stiffness, in this case showed the opposite trend to the elastic modulus with PEGDA 258 at 2.03±0.99 N/m, PEGDA 575 at 1.68±0.88 N/m and finally PEGDA 700 at 1.48±0.53 N/m.

5.1.3.1 PPP-ZEIHR Cantilever

Most of the work was performed using the AC160 cantilever (k = ~40 N/m). Therefore, it was essential to the use of another cantilever is important for comparison. Nanoindentation experiments were therefore conducted using a softer cantilever with a nominal force constant ~

20 N/m (PPP-ZEIHR. Each cantilever was calibrated to obtain the precise values of the spring constants associated with each cantilever. To confirm the values provided by the manufacturer we measured the spring constant of every cantilever on a hard and clean mica surface as described earlier. It is important to note that the thermal fluctuation method used to calibrate the cantilever has a significant error associated with it that also propagates in calculation of the mechanical properties of the material of interest [75]

	HIGH LOAD		HIGH DISPLACEMENT	
	PEGDA 575		PEGDA 575	
	PPP-ZEIHR	AC 160	PPP-ZEIHR	AC 160
Ec (avg) Mpa	1.61	0.81	1.83	1.46
Stiffness (avg) N/m	1.18	0.82	1.11	0.6

Table 11 Elastic modulus and stiffness of PEGDA 575 using two different cantilevers

Table 11 shows the calculated elastic modulus for the PEGDA 575 samples using PPP-ZEIHR cantilever (k = 18.1 N/m (high load) and 17.4 N/m (high displacement)). It may be noted that the value was slightly different from the one using the AC 160 cantilevers (k = 31.7 N/m for both high load and displacement). Under both high load and high displacement indent modes, the elastic modulus values of the PEGDA 575 using PPP-ZEIHR were higher in value (1.61±0.10MPa, 1.83±0.03MPa) as well as the stiffness (1.18±0.01 N/m, 1.11±0.06 N/m). On the other hand using AC160, the values were lower 0.81±0.02 MPa and 1.46±0.07 MPa for the elastic modulus, 0.82±0.04 N/m and 0.60±0.06 N/m for the stiffness (Table 11). Due to the inherent inaccuracy in determination of the spring constant, these values are not considerably different. While attempts were made to use this cantilever in under low loads and low displacement, the extremely high noise in the data precluded any meaningful analysis. This may

be attributed to the softer nature of the cantilever. In Figure 24 both graphs representing high load and displacement indent mode respectively are shown. Since the curves were normal and clear with minimal noise, it was easy to fit the Oliver-Pharr model and data was obtained.

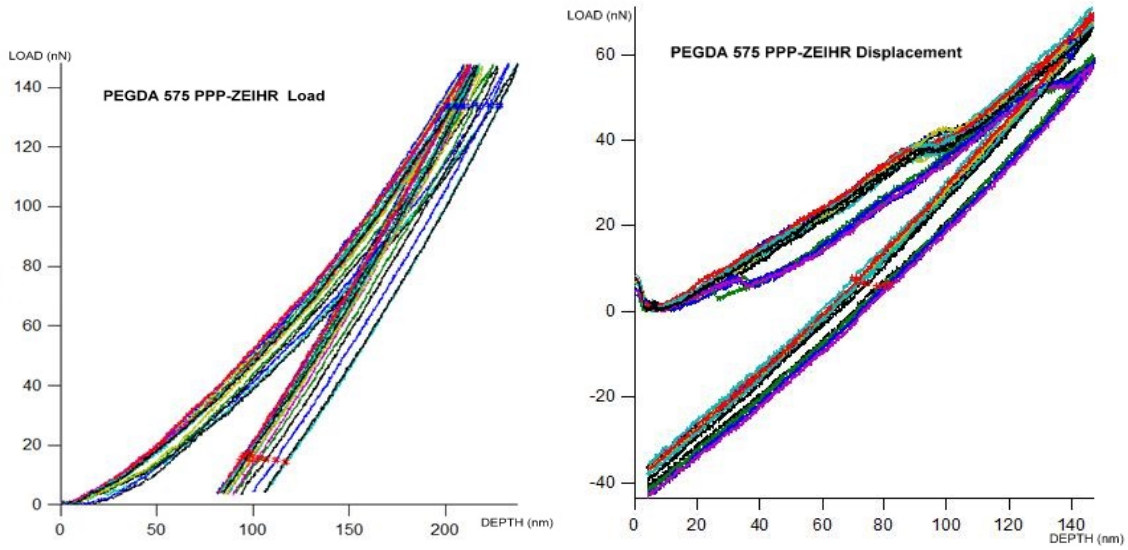

Figure 24 Indentation curves using PPP-ZEIHR cantilever under high load and displacement for PEGDA 575 hydrogel

5.1.3.2 Variation of the initiator composition

As mentioned earlier, three different PEGDA 575 hydrogels were fabricated with varying amounts of initiator, and then tested. The objective of these experiments was to determine the effect of the initiator in determining the final crosslinking of the diacrylate monomer (Figure 3). The hydrogel samples were tested using 0.5 %, 1% and 1.5 % initiator v/v. The nanoindentation experiments were all performed in dry condition with only using the AC160 cantilevers. Table 12 summarizes the elastic modulus and stiffness average values obtained after fitting the unloading part of the curves with Oliver-Pharr model. The elastic modulus of the three PEGDA

575 hydrogels increased in value (from 3.66 MPa (1% initiator) to 12.12 MPa (1.5% initiator)) with increasing the amount of the initiator in the PEGDA mixtures. The same behavior was observed for the stiffness as well (from 1.95 N/m (1% initiator) to 4.85 N/m (1.5% initiator)).

	PEGDA 575, Dry condition		
	0.5 % initiator	1 % initiator	1.5 % initiator
	AC 160, Sp.cst 46.81 N/m	AC 160, Sp.cst 37.91 N/m	AC 160, Sp.cst 42.72 N/m
Ec (MPa)	3.66	4.33	12.12
Stiffness (N/m)	1.95	2.48	4.85

Table 12 Elastic modulus and stiffness average values for the different PEGDA hydrogels (dry condition)

5.1.4 Wet condition

Performing nanoindentation experiments on hydrated hydrogel surfaces is of great interest. Two cases were investigated with 63% and 86% partially hydrated PEGDA 575 samples. A few curves that could be fit with the Oliver-Pharr model were obtained and analyzed. Figure 25 show the indentation curves that were obtained with 86% water and Figure 26 shows the indent curves obtained with 63% water.

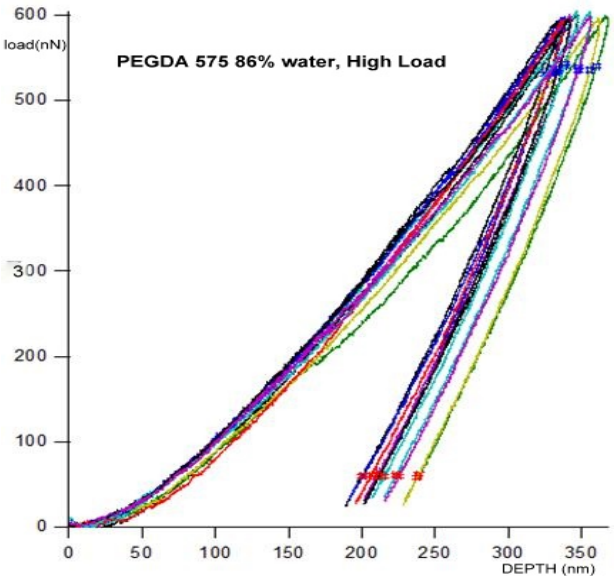

Figure 25 Nanoindentation curves of the PEGDA 575 with 86% water that were analyzed

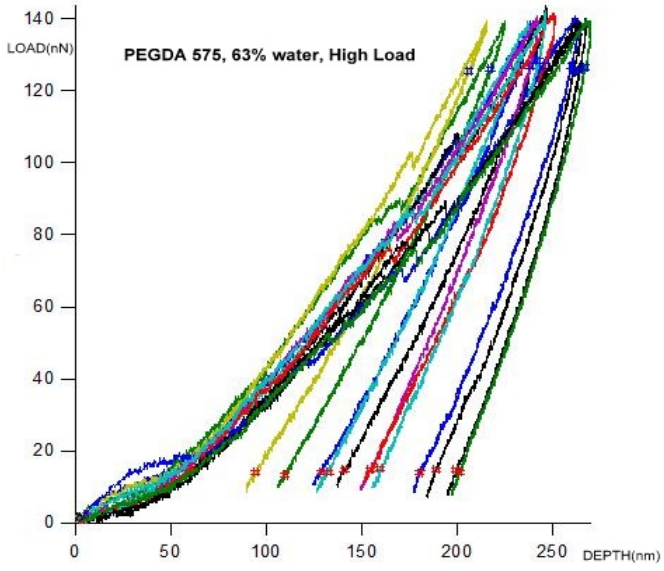

Figure 26 Nanoindentation curves of the PEGDA 575 with 63% water that were analyzed

	HIGH LOAD	
	PEGDA 575	
	63%	86%
Ec (avg) Mpa	4.33	2.85
Stiffness (avg) N/m	2.48	4.32

Table 13 Elastic modulus E_c and stiffness S average values in partially wet conditions

Under high load indent, the PEGDA 575 sample with less water content 63% had a higher elastic modulus 4.33±0.28 MPa and a higher stiffness of 2.48±0.27 N/m. However, with 86% water, the PEGDA 575 elastic modulus dropped to 2.85±0.35 MPa, while the stiffness increased to 4.32±0.12 N/m. Since the values for elastic modulus and stiffness are exactly the same for PEGDA 575 (1% initiator) in dry condition as well as in 63% water condition (4.33 MPa and 2.48 N/m), it is likely that the indentation was performed on a dry surface. While the bulk water content is ~63%, blowing the surface with air might have resulted in a dry layer of the hyrogel sample (several hundred nanometers deep).

To minimize such errors in hydration and also since a fully hydrated hydrogel mimics a real-life application, it was important to measure the nanomechanical properties of the hydrogel in a fully hydrated state. This was attempted by performing the nanoindentation experiments under water. This experiment was particularly challenging given the limited control of the experimental parameters when the indenter is used under water. Notice that only PEGDA 575 with 1% initiator was used under wet condition. After several unsuccessful trials, it was observed that data was only obtainable using the AC160 cantilever due to its high spring constant and stiffness. The softer PPP-ZEIHR was not well suited for such complicated and challenging experiments. It was also extremely difficult to obtain a well attached hydrogel sample that could be investigated. Furthermore, higher thermal fluctuations in the water result in higher drift in the

x, y and z directions making the experimental data extremely noisy. Consequently, data was obtained only for high displacement and high loading for this condition. In the Table 14 below, the summary of indentation experiments under high load and displacement indent modes, using two different AC160 cantilevers with different spring constants 43.57 N/m (high load) and 31.7 N/m (high displacement) is presented,. Under high load indent mode, the elastic modulus was 1.04±0.09 MPa, but under high displacement indent mode the elastic modulus is almost 8 times higher at 8.32±0.71 MPa. The stiffness values in both modes were not far apart with 2.83±0.07 N/m (high load) and 2.55±0.71 N/m (high displacement).

	PEGDA 575	
	High Load	High Disp.
Ec (avg) Mpa	1.04	8.32
Stiffness (avg) N/m	2.83	2.55

Table 14 Elastic modulus E_c and stiffness S average values of PEGDA hydrogel under water

5.1.5 SEM imaging of the AFM cantilever:

Since one of the key parameters in determining the accuracy of our fit is the tip geometry, it was important to confirm the morphology of the cantilever prior to and after the indentation experiments. The purpose of the latter step is to determine the effect of the indentation on the geometry of the tip as a result of these experiments. A scanning electron microscope was used to obtain images of the AFM cantilever tip. The first set of images was taken before the nanoindentation experiments. Figure 27 shows a clean AC160 cantilever with no surface impurities or imperfections. It is important to notice the sharpness of the edges and the geometry of the tip; tetrahedral shape. After the nanoindentation experiments were done, another set of SEM images were obtained of the cantilevers used to determine if the experiments resulted in

any tip damage. Figure 28 shows that cantilever tip picked up some of the hydrogel debris. In Figure 28 (right image), the probe appears to have lost its sharpness resulting in a slightly curved edge. It is important to note that these irregularities in the geometry of the tip can affect the spring constant calculations and also the parameters used in the analysis of the nanoindentation curves. These sources of error may result in a wide variation in our fit and are discussed in the next section.

Figure 27 AC 160 cantilever before the nanoindentation experiments

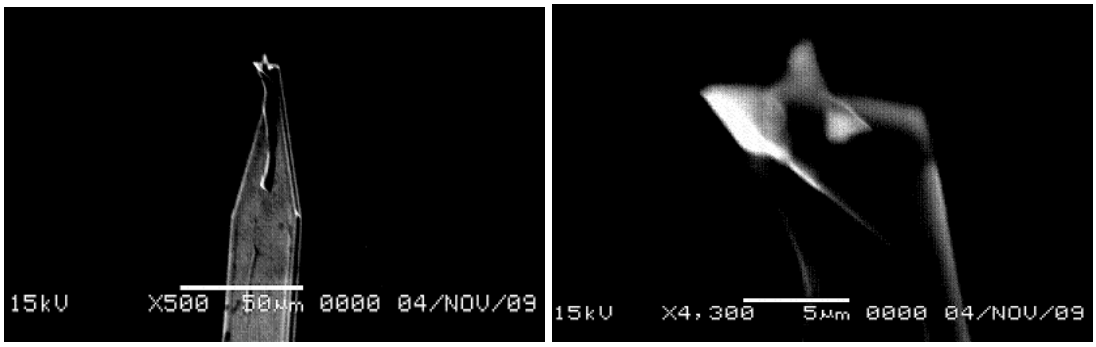

Figure 28 AC 160 cantilever after the nanoindentation experiments

5.2 Discussion

5.2.1 Problems with formation of polymer

After the PEGDA samples were polymerized, they were washed and then dried. During this last procedure, some irregularities were noticed within the samples. Cracks and deformations were observed, especially after the drying step. In water, the polymer network swells causing the conformation of the polymer chains to change resulting in molecular stretching and disorder within the polymer. At a higher level of hydration the hydrogel materials become more sensitive to defects and crack propagation and possibly mask molecular level phenomena [89]. Once these samples were placed in the oven for drying, the rate of heating was fast, causing the molecules to re-orient and based on extensive fracture of their chemical bonds, cracks were observed (Figure 29).

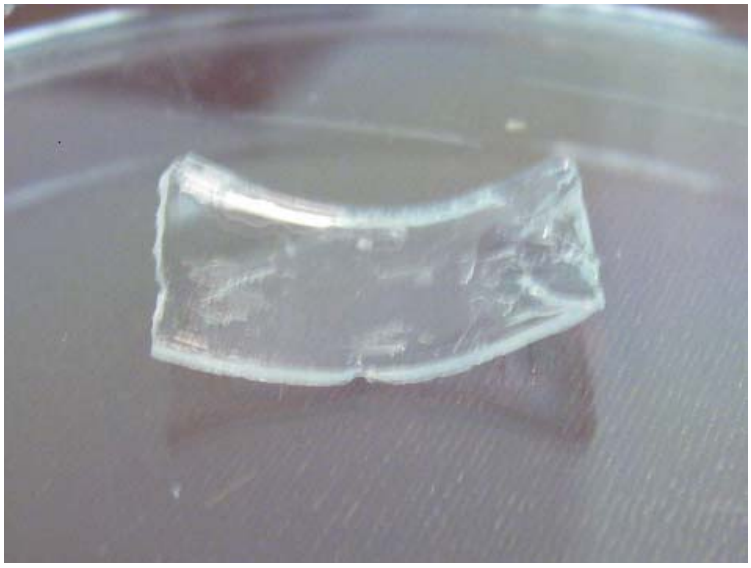

Figure 29 A deformed PEGDA hydrogel sample showing crack propagation

5.2.2 Nanoindentation using the Hysitron® instrument

Initially, to compare our results obtained using AFM-based nanoindentation, we tried to investigate the mechanical properties of PEGDA hydrogels using another instrument, the *Hysitron® Ubi1 Nanoindenter*. The main difference with this machine compared to an AFM is that the nanoindentation performed is in a destructive fashion. This instrument uses a standard diamond coated Berkovich indenter with a much higher modulus compared to the sample of interest. In contrast, our AFM experiments used a softer silicon nitride cantilever to probe the surface non-destructively. Therefore, the comparison of the mechanical properties of PEGDA under both approaches is of great interest. The primary challenge with the Ubi1 instrument was its calibration. It is imperative to perform the necessary calibrations in order to maintain the precision and accuracy of the instrument while performing imaging and data analysis.

However, these initial attempts proved to be unsuccessful. The problem consisted mainly in the form of vibrational noise in the surrounding environment caused by the ventilation system in the room. This resulted in a high perturbation within the system and an even higher noise in the calibration procedure. Figure 30 presents an actual trial of the calibration. In the upper right corner of the figure, ESF (Electrostatic force) vs. Displacement graph shows unstable and noisy plot, compared to the usual ESF vs. Displacement plot with a reasonable fit provided by the *Hysitron®* manufacturer (see Figure 31). Figure 31 represents the case where the calibration was complete and the system ready for operation. Because of these calibration issues, we did not perform any further experiments using this instrument

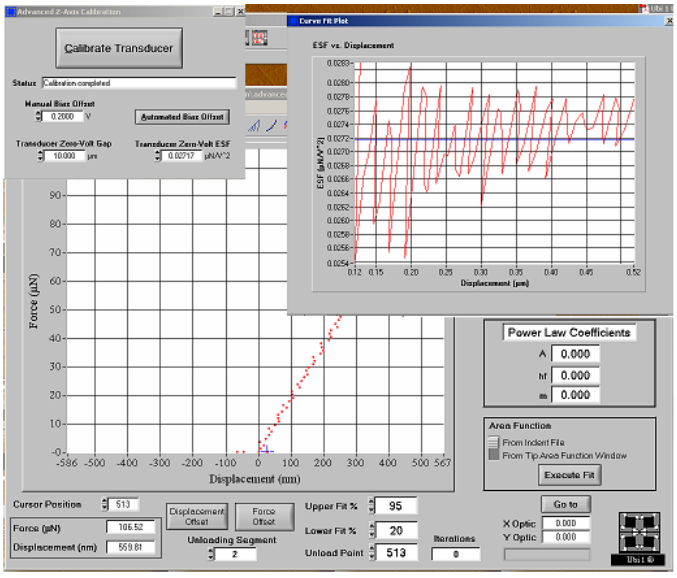

Figure 30 Calibration of the Ubi1 nanoindenter in air (the Advanced Z-Axis Calibration)

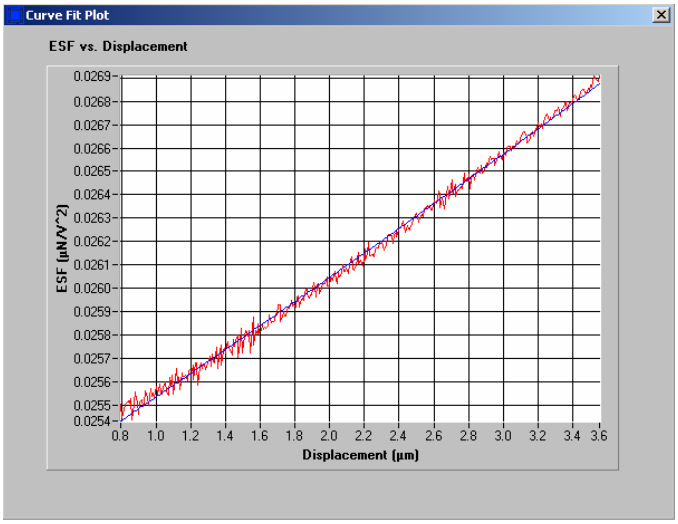

Figure 31 Normal ESF vs. Displacement plot *(Hysitron®)*

5.2.3 Nanoindentation via AFM

As mentioned in the sections above, nanoindentation was performed in four different modes – high and low load and displacement. The high load indent mode was the most used

mode throughout the course of this research and resulted in the highest signal to noise ratio for the force-displacement curves analyzed. The low indent mode was used but only in the dry condition and with the stiffer AC160 cantilever. Under low displacement indent mode, the tip interaction with the PEGDA surface became significant (the force applied is around 50 nN and depth traveled around 100nm or less) which made the softer cantilever with small spring constant values (PPP-ZEIHR) incapable or not well suited to perform indentation tests. For example in Figure 32 the unloading trace of the load-displacement curves at low displacement using an AC160 cantilever are shown. The high noise made the analysis more challenging and the results difficult to interpret and fit via the models discussed.

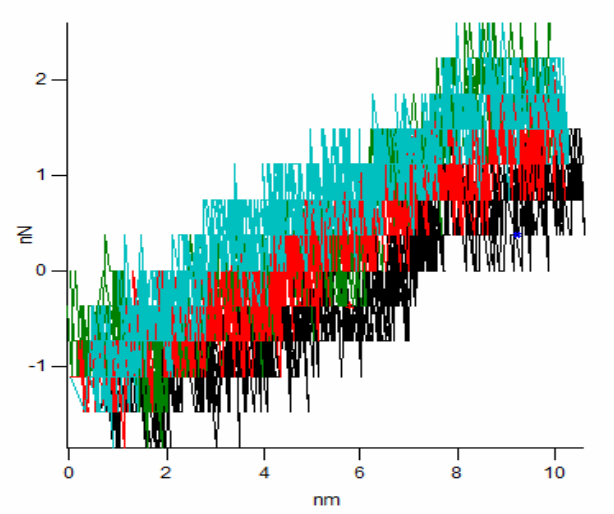

Figure 32 Unloading part of the nanoindentation curve

5.2.3.1 Load indent mode

Elastic modulus and stiffness of the PEGDA hydrogels

Nanoindentation results obtained for the hydrogel samples were presented in the previous chapter. All the PEGDA in the subsequent discussion were made with 1% initiator v/v.

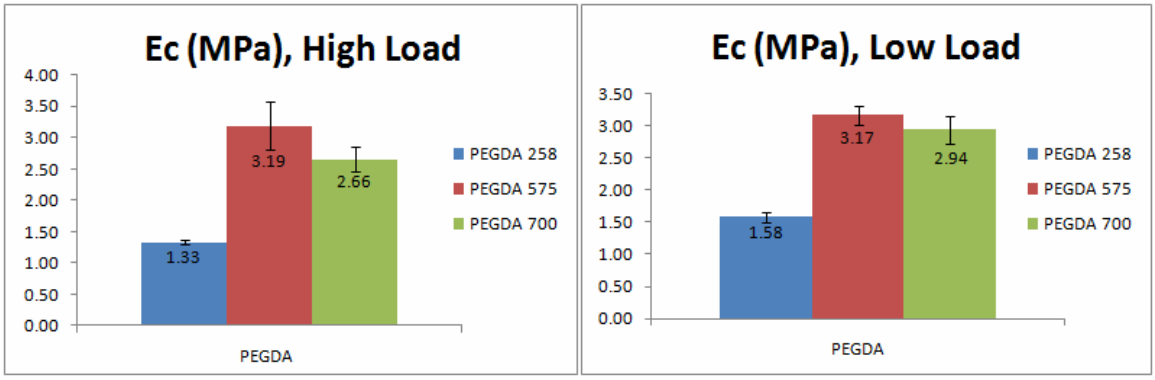

Figure 33 PEGDA Elastic modulus E_c under load indent mode

With higher molecular weight, the PEGDA hydrogel has shown in increase in elastic modulus. Under high load the PEGDA 575 shows higher elastic modulus as well as under low load indent mode. The standard deviation was a marginally higher for the high load. The variation in the values of the modulus at different points on the hydrogel surface was low indicating that the surface was uniform. The PEGDA 700 elastic modulus did not show a difference in either mode. The PEGDA 258 hydrogel has the lowest elastic modulus with only 1.33 and 1.58 MPa under high and low modes respectively. Here, the molecular weight difference is observed to affect the performance of the hydrogel. In Figure 33, the average elastic modulus distribution was about the same in both indent modes (high and load). This is reasonable, because in the case of PEGDA 258 for example, by applying a load of 150 nN, the tip traveled around 60 nm more than for a 20nN force. The same situation was observed for the stiffness values. PEGDA 575 and 700 hydrogels had a higher stiffness value in comparison to PEGDA 258, which may represent a weaker material.

Under higher load indent, the PEGDA 700 hydrogel had a higher stiffness value. Figure 34 shows that the stiffness dropped by half under low load indent mode. When a load of 200 nN

is applied, the tip travels ~300 nm into the surface. On the other hand, at a low load of 20 nN, the tip travels ~200 nm into the surface. This implies that a tenfold increase of load does not result in a proportional increase in penetration.

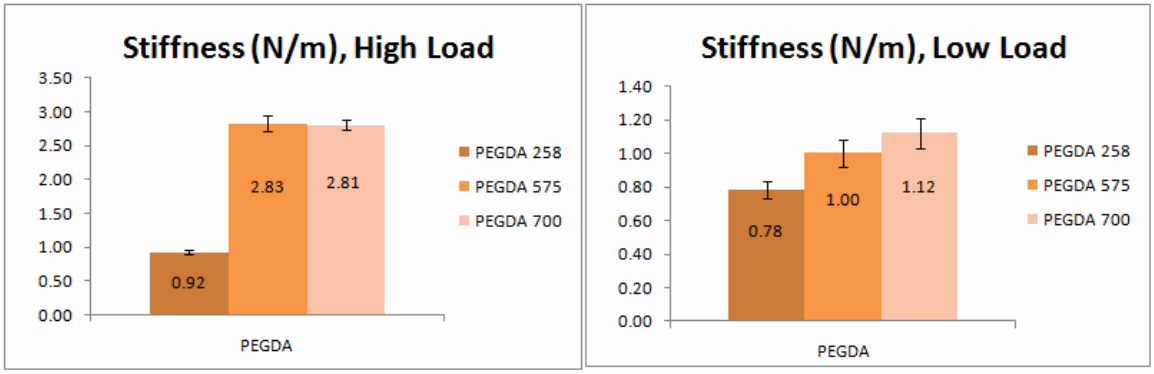

Figure 34 PEGDA stiffness *S* under load indent mode

Wet condition

Experiments to conduct nanoindentation in liquid were extremely challenging. The first problem consisted of fixing the PEGDA hydrogel sample on the glass slide, by keeping it under water for long time to attain its maximum swelling and to ensure thermal equilibration with the AFM cantilever. During this long process under water, the PEGDA sample started to detach from the glass slide, and floated away in the liquid cell, making the nanoindentation impossible. Several trials later, limited data was obtained for analysis because of this problem. In addition, the PPP-ZEIHR cantilever was too soft to accurately image the surface or perform indentations owing to the strong tip-surface adhesion. In order to obtain indentation data under water, it was necessary to use the stiffer AC160 cantilever (k=~40 N/m). Under high load conditions, the 63% PEGDA 575 elastic modulus was the highest, followed by 86% and 100%. Therefore by

increasing the water content in PEGDA 575, the elastic modulus decreases as expected. Figure 35 shows clearly the drop in elastic modulus with increasing the percent hydration.

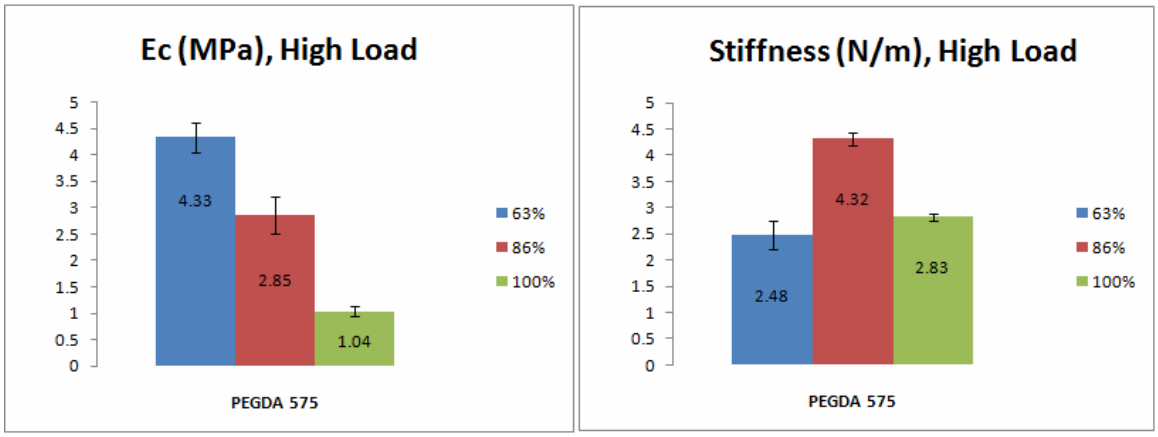

Figure 35 Partially and fully hydrated PEGDA elastic modulus E_c and stiffness S measurements under load indent mode

5.2.3.2 Displacement indent mode

Controlling the displacement while indenting on the PEGDA surfaces, was more challenging than controlling the load, especially at low displacements. Performing nanoindentation under water using the low displacement mode was difficult and no data was recorded. As observed with load indent, the use of the PPP-ZEIHR cantilever under water was not possible since the force interaction and the thermal fluctuation within the liquid was significant. On the other hand, this cantilever was useful for experiments in the dry condition and under high displacement indent mode.

The elastic modulus measurements under high displacement indent mode were slightly different from the high load experimental values (Figure 36). An identical trend of the elastic modulus to molecular weight relation was observed. The higher molecular weight corresponds to

a higher elastic modulus in both high load and displacement indent mode. However, the low displacement measurements of the elastic modulus were observed to have extremely high noise levels. This was expected because the tip penetration into the sample was only ~ 10 nm. The elastic modulus values were above 40MPa as shown in Figure 36 (right), the same trend about the molecular weight and the elastic modulus relation is observed as well. But the higher values may be because of large errors in fitting the data, as discussed further below.

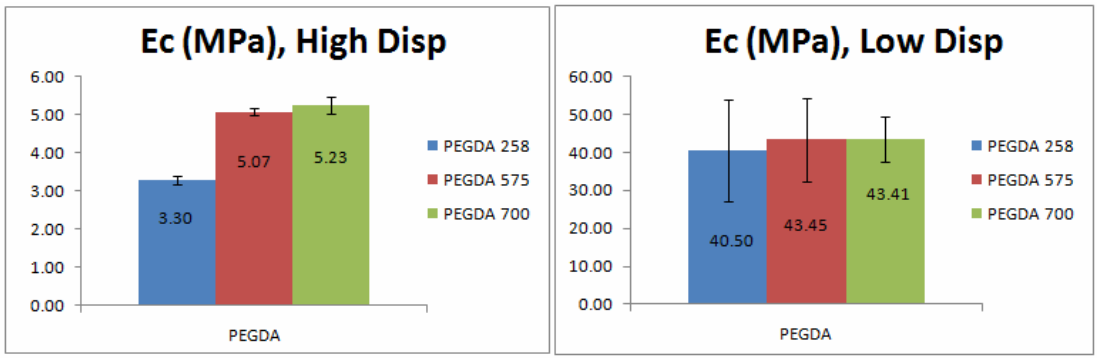

Figure 36 PEGDA elastic modulus E_c under displacement indent mode

The stiffness measurements of the different PEGDA were almost the same under high displacement. PEGDA 575 was the stiffest material while the PEGDA 258 was the least stiff among these three hydrogels (Figure 37, left diagram). On the other hand, the low displacement in Figure 37 (right) showed practically the opposite trend. PEGDA 258 was stiffer among other PEGDA hydrogels but the PEGDA 575 and 700 stiffness values remained about the same in both displacements mode. Here, again the low displacement indent mode showed difference in the stiffness measurements as well. This can be related to the chain confirmation of the polymer at the surface of PEGDA 258.

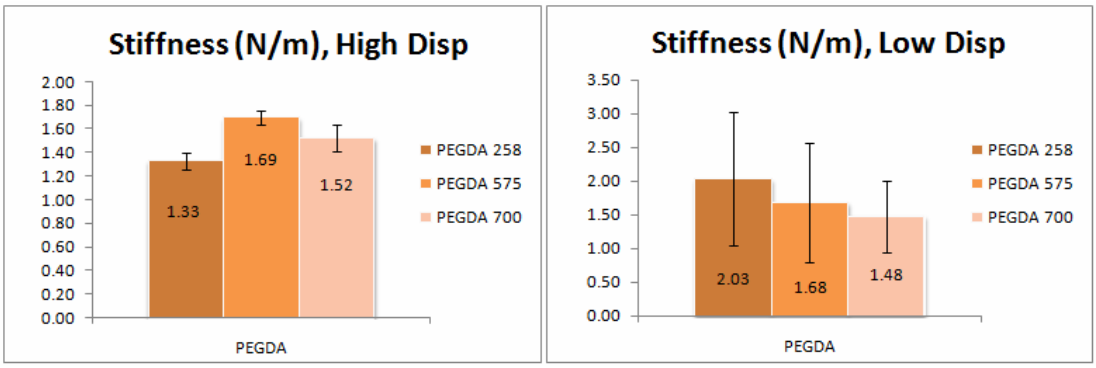

Figure 37 PEGDA stiffness *S* under displacement indent mode

5.2.4 Hydrogel mechanical properties in comparison to other materials of biological significance

Since PEGDA 575 was the most stable throughout the fabrication procedure and the indentation experiments, it was chosen to be compared with other materials. The average elastic modulus varied between 2 to 5 MPa under different conditions. Table 15, shows the measured elastic modulus of PEGDA under different condition and methods, tabulated from Gäbler et al. [90]. It was of interest to note that the typically calculated value of 3.5 MPa was in the range of the interval values provided in the table below.

The elastic modulus is one of the most common properties used to characterize the mechanical behavior and describe the material. For example, by measuring the modulus of soft hydrogel polymers, Wilder et al. have found that by varying the crosslinking concentration in the Poly (HEMA) hydrogel the elastic modulus increased from 0.56±0.06 MPa (0.5% initiator) to 2.6±0.51 MPa (8% initiator) [91]. In a review of elastic moduli of several soft biological materials by Levental et al. [46], the elastic modulus measurements of a variety of tissues such as animal and human tissue were given. For example, using a tensile method, the elastic modulus of

an Achilles' tendon of a rat was around 310 MPa, which is a much higher than our PEGDA samples. Typical values for soft mammalian tissues ranged from ~ 100 Pa for brain tissue to several thousand for muscle tissue. The elastic modulus of a mouse skeletal muscle using AFM was ~13 KPa, which is a lot smaller than the PEGDA elastic modulus. The elastic modulus of a human breast tumor tissue using compression was about 4 KPa, which is even smaller than the mouse's skeleton muscle elastic modulus.

Sample	PEG-DA ma%	Nanoindentation (MPa)	mI:cyl (MPa)	mI:sph (MPa)	Compression (Mpa)	DMA (Mpa)
46-2	39.4	3.29±0.17	5.23±0.24	6.66±0.92	3.19±0.16	8.68
47-2	32.9	N/A	5.08±0.07	6.44±0.098	2.84±0.006	8.16
49-4	32.8	2.81±0.29	3.55±0.02	3.35±0.152	2.60±0.16	6.16
48-1	30.5	3.03±0.38	3.73±0.10	4.60±0.032	2.28±0.009	5.16
45-1	27.1	2.65±0.07	1.76±0.012	2.6±0.055	2.15±0.004	3.04
44-1	22.8	2.04±0.04	1.04±0.008	1.44±0.007	1.26±0.014	1.43
43-3	14.9	N/A	0.32±0.003	0.57±0.006	0.44±0.005	0.41
35-4	12.6	1.84±0.06	0.14±0.003	0.12±0.016	0.22±0.004	0.19
36-3	7.1	N/A	0.03±0.001	N/A	0.05±0.002	0.04

Table 15 Summary of the elastic moduli of PEG-DA hydrogels as measured with different measuring methods (adapted from [90])

In order to apply these hydrogels for tissue engineering and scaffolding, it is necessary to control the mechanical properties hydrogel matrix. Here we show that by varying parameters such as molecular weight, initiator concentrations and hydration rates, it is possible to control properties such as the elastic modulus at the nanoscale. This is particularly significant, to achieve properties similar to biological tissues and mimic the mechanical behavior of real tissues *in vivo*, thereby controlling cell behavior and fate.

5.2.5 Sources of error:

It must be noted that the values reported in this research are subject to a lot of variation and significant sources of error. These sources are discussed below:

5.2.5.1 Accuracy in measuring the spring constant

Most AFM experiments require accurate knowledge of cantilever spring constants in order to image or measure both force-distance and indentation curves. Due to the challenges faced while controlling the thickness, the structural defects and deviations in geometry, the manufacturers of AFM cantilevers use wide tolerances in their specified values of the spring constant [92]. Therefore, re-calibration of the cantilever tips is mandatory before usage.

There are several method designed to measure the spring constant, including using the actual geometry of the tip. Here, again many approximations were taken into account due to the difficulty of obtaining the exact dimensions of the indenter. Thermal fluctuation is a another method that has been used throughout this research, it consists of calibrating the cantilever with thermal noise which is affected by several factors including the laser intensity and spot position on the cantilever, in addition to its size [75]. That is why it is important to repeat the spring constant calibration of the cantilever several times to finally obtain an average value. This might minimize the error experimentally as well as in the data analysis. However, these and other methods to estimate the spring constant of the cantilever are subject to large variations, sometimes on the order of 50% in the calibration values. These variations may result in wide ranges for the forces and therefore the elastic moduli and stiffness values calculated.

5.2.5.2 Tip geometry

In nanoindentation experiments, the geometry of the indenter plays a big role in measuring the mechanical properties of the material of interest. The change in the tip radius of curvature, for instance, can significantly affect the experimental results (imaging and force-distance analysis) [93]. It can also affect the indentation and penetration process as well as the

analysis since the indenter will deform the sample with different geometry. In the case of the AC160 cantilever used throughout the nanoindentation experiments, a tetrahedral geometry was assumed as discussed below. Our calculations implicitly assume that the tip geometry is not altered as a result of the indentation experiments. As shown in the SEM images (Figure 28) in several cases, the cantilever loses its initial sharpness as expected, becoming a little blunt and contaminated with the hydrogel as well. These factors may result in a further loss of accuracy in our experiments.

5.2.5.3 Tip surface interaction

Tip surface interaction and especially the non-specific interactions (circled in green in Figure 38) provide another important source of error. At the nanoscale, the Van der Waals forces become more significant, resulting in adhesion between the cantilever and the surface investigated. This is manifested in the retraction trace of the force-displacement curve that can be seen in Figure 38.

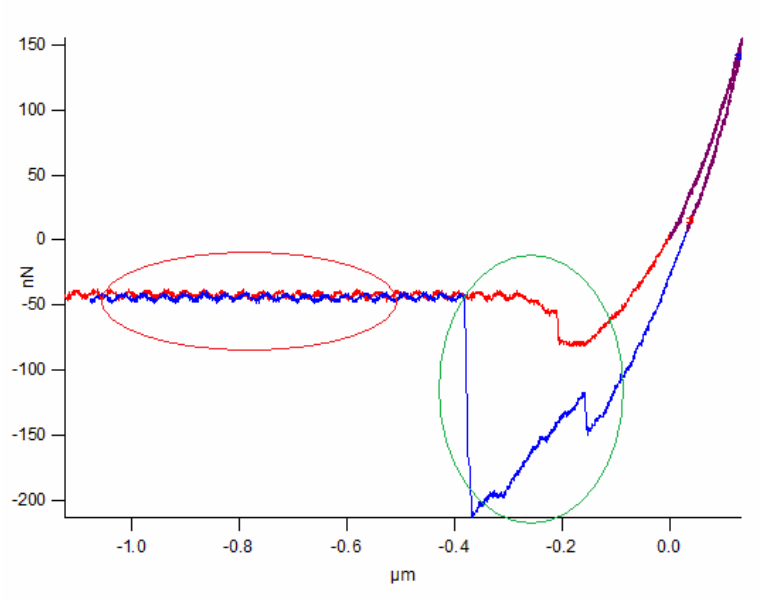

Figure 38 Indent view of a force-distance curve showing a high degree of non-specific tip-surface interaction (green circle). The red circle represents vibrational noise as the cantilever retracted away from the surface. However, the indent portion of the curve was not affected as the tip traveled at the surface under the high load

Even though the tip-surface interactions were significant in some cases, the tip did not stick to the sample during the nanoindentation step, resulting in reasonable curves that were well fit with the Oliver-Pharr model, especially at high load and displacement. However, to reduce any possible errors, it is important to investigate strategies to try and minimize non-specific adhesion between the tip and the surface.

Finally, we look at the inherent assumptions in the models associated with the fitting of the experimental that may also result in some error.

5.2.5.4 Hertz model fit

Despite the fact that it is best used for rigid materials, the Hertz model was initially used to fit the nanoindentation curves of the PEGDA samples. However, it was really challenging to estimate the geometry of the indenter. The closest shape available to a tetrahedral structure is a cone geometry. In addition the half cone angle needed to be determined prior to analysis. In Figure 39, an attempt to fit a PEGDA indentation curve to the Hertz model is presented. By using the estimated value of the half cone angle, the model could not fit the data provided. To actually fit the curve, we had to keep changing the half angle contact values until a reasonable fit was obtained. It was observed that the fit was somewhat arbitrary since changing the half-angle resulted in better fits of the data. However, this value did not reflect the actual geometry of the tip.

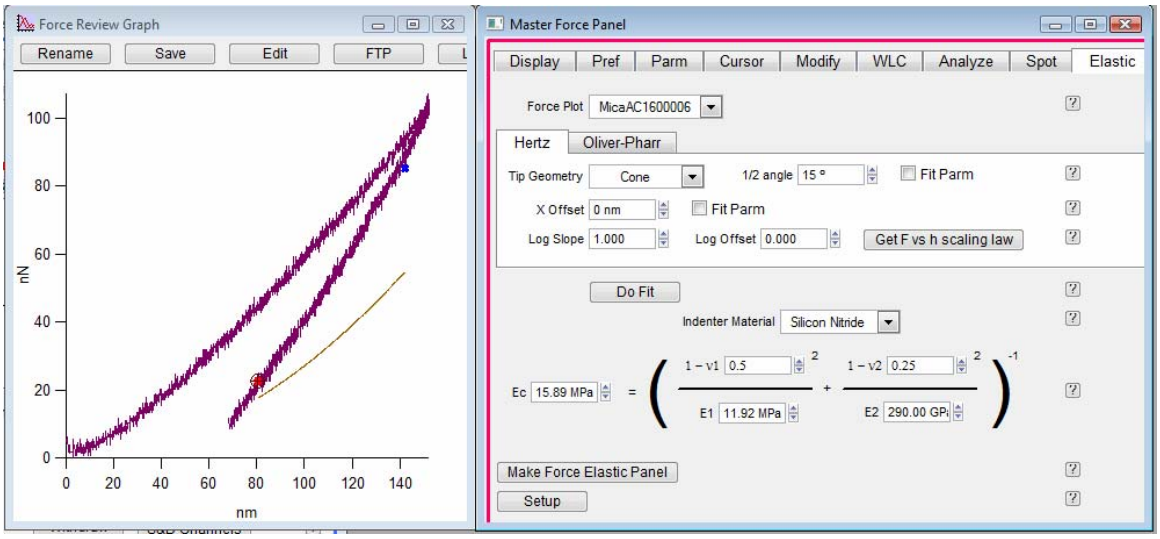

Figure 39 Hertz model fit of a nanoindentation force curve

After several trials, we were convinced that without the exact dimensions and the shape of the tip the analysis would be full of error. We then used Oliver-Pharr as the primary model to fit the nanoindentation curves of the PEGDA hydrogel.

5.2.5.5 Inherent errors in measurement using the Oliver Pharr model

Oliver-Pharr model was the best model to fit our nanoindentation data. However, there are several sources of inaccuracy in the determination of the elastic modulus using this model as well. The main problem consisted of attempting the fit from the unloading trace of the nanoindentation curve. This was typically significant while analyzing under low displacement indent mode data (Figure 40). By slightly changing the positions of the cursors used to fit the data, a large difference in the elastic modulus value could be observed. It is important to note the difference in value of the elastic modulus (from 704.77 kPa to 17.4 MPa) could be obtained from the same curve as shown in Figure 40 This degree of subjectivity may have resulted in some error in our calculations. It must be noted, that the differences were not as significant in the higher displacement or load experiments. In addition, the contact area A_c used for calculating the elastic modulus in the Oliver-Pharr model is for a Berkovich tip which has a tetrahedral geometry and described by:

$$A_c = 24.5 * H^2_c$$

where H_c is the contact height (Figure 9).

From the SEM images of the AC160 tip, it was observed that contamination as well as a change in geometry of the contact area may occur as a result of these experiments. These

inherent sources of error indicate that the tip geometry must be accurately quantified prior to analysis of the force-displacement curves measured.

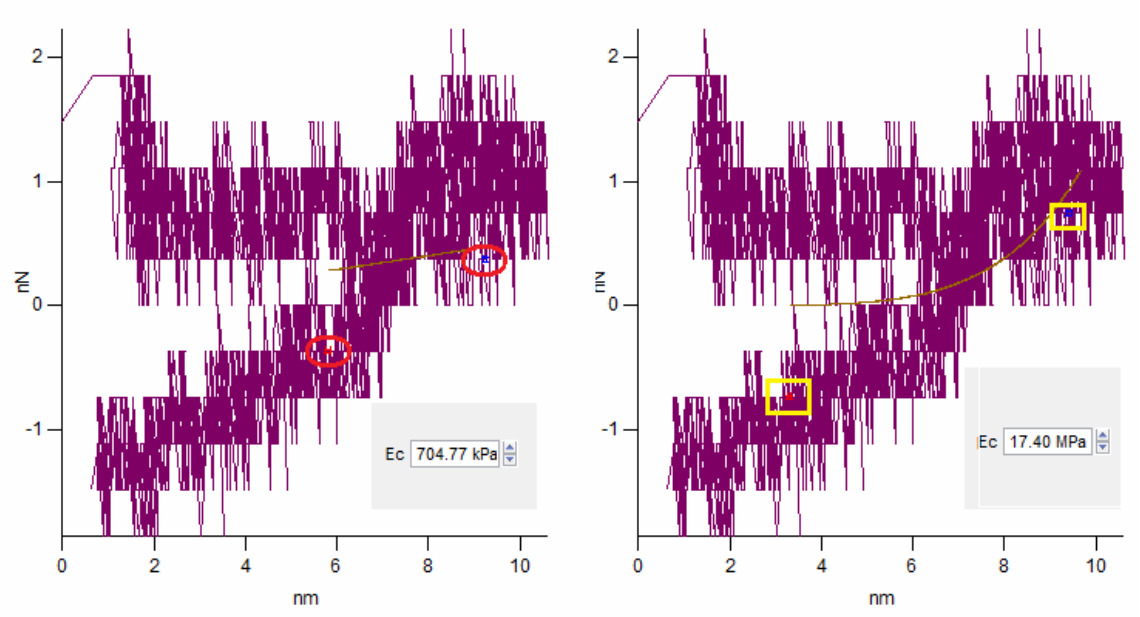

Figure 40 The influence of the position of the cursors on a low displacement nanoindentation curve using the Oliver-Pharr model. By slightly changing the positions of the cursors in the red circles (left curve) to a slightly different positions in the yellow rectangles (right curve) to fit the data, a large difference in the elastic modulus value was observed

Chapter 6: Conclusion and Future Work

While the mechanical behavior of hydrogels has been estimated at the bulk scale, there have been limited studies at the nanoscale. In this research, we investigated the mechanical properties of PEGDA hydrogels at the nanoscale by measuring the elastic modulus as well as stiffness via nanoindentation using an AFM. We showed that the silicon nitride cantilevers can be used to perform nanoindentation, particularly at higher loads and displacements. The mechanical behavior of PEGDA hydrogels was observed to depend on many parameters including the water content, monomer molecular weight, photoinitiator concentration and photopolymerization procedure.

By increasing the amount of the crosslinking agent, the elastic modulus as well as stiffness increased in value. It was observed that the higher the molecular weight of the hydrogel, the higher is the value of the elastic modulus. These experimental and analysis parts were studied under high load and displacement indent modes. At lower displacement indent mode (~10nm) and load indents, the tip-surface interaction forces were predominant led to high error, which made analysis difficult. Stiffer cantilevers with a higher spring constant were found to work better to get force-displacement curves that could be easily analyzed.

Two models were compared to fit the data- Hertz and Oliver-Pharr. The classical Hertz model was used first since it is the most prevalent. The analysis using this model is mostly based on accurately determining the geometry of the indenter (cantilever tip). In addition, the Hertz theory is based on performing the indentation on rigid surfaces. The PEGDA hydrogels, as soft materials required the Oliver-Pharr model as best suited for our experiments. Scanning electron microscopy was introduced in the scope of the research to confirm the geometry of the tip before and after the indentation. Some images taken of the cantilever revealed that cantilever geometry

does indeed change as a result of nanoindentation and tips are also likely to be contaminated with the sample.

Since most application of hydrogels are in biomedical fields such as drug delivery and tissue engineering, calculating and controlling the mechanical properties of a hydrated polymer is of great interest. Therefore investigating the mechanical properties of PEGDA hydrogel in liquids is the next important step. Even though it has been done in this research, further studies are encouraged to confirm the results obtained. The determination of the indenter structural shape and physical properties is really important in the characterization of the material of interest. In addition, the choice of the material of the indenter (cantilever tips) is important as well, to minimize the non-specific interaction with the surface indented. In future studies, better models and methods should be developed to identify the mechanical properties of soft material via nanoindentation experiments. The development consists of studying and confronting the challenges faced with indenter properties and geometry as well as minimizing the error obtained from the non-specific force interaction, in addition to determine the indentation material parameters for contact modeling, stress/strain analysis and load bearing.

References

1. Nguyen, K.T. and J.L. West, *Photopolymerizable hydrogels for tissue engineering applications.* Biomaterials, 2002. **23**(22): p. 4307-4314.
2. Holtz, J.H. and S.A. Asher, *Polymerized colloidal crystal hydrogel films as intelligent chemical sensing materials.* Nature, 1997. **389**(6653): p. 829-832.
3. Khademhosseini, A. and R. Langer, *Microengineered hydrogels for tissue engineering.* Biomaterials, 2007. **28**(34): p. 5087-5092.
4. Miyata, T., N. Asami, and T. Uragami, *A reversibly antigen-responsive hydrogel.* Nature, 1999. **399**(6738): p. 766-769.
5. Van Tomme, S.R., G. Storm, and W.E. Hennink, *In situ gelling hydrogels for pharmaceutical and biomedical applications.* International Journal of Pharmaceutics, 2008. **355**(1-2): p. 1-18.
6. Ladet, S., L. David, and A. Domard, *Multi-membrane hydrogels.* Nature, 2008. **452**(7183): p. 76-U6.
7. Nicolson, P.C. and J. Vogt, *Soft contact lens polymers: an evolution.* Biomaterials, 2001. **22**(24): p. 3273-3283.
8. Ulijn, R.V., et al., *Bioresponsive hydrogels.* Materials Today, 2007. **10**(4): p. 40-48.
9. Jeong, B., S.W. Kim, and Y.H. Bae, *Thermosensitive sol-gel reversible hydrogels.* Advanced Drug Delivery Reviews, 2002. **54**(1): p. 37-51.
10. Ahearne, M., et al., *Characterizing the viscoelastic properties of thin hydrogel-based constructs for tissue engineering applications.* Journal of the Royal Society Interface, 2005. **2**(5): p. 455-463.

11. Calvert, P., *Hydrogels for Soft Machines.* Advanced Materials, 2009. **21**(7): p. 743-756.

12. Swann, J.M.G. and A.J. Ryan, *Chemical actuation in responsive hydrogels.* Polymer International, 2009. **58**(3): p. 285-289.

13. Ratner, B.D. and A.S. Hoffman, *SYNTHETIC HYDROGELS FOR BIOMEDICAL APPLICATIONS.* Acs Symposium Series, 1976(31): p. 1-36.

14. Kopecek, J., *Hydrogel biomaterials: A smart future?* Biomaterials, 2007. **28**(34): p. 5185-5192.

15. Buxton, A.N., et al., *Design and characterization of poly(ethylene glycol) photopolymerizable semi-interpenetrating networks for chondrogenesis of human mesenchymal stem cells.* Tissue Engineering, 2007. **13**(10): p. 2549-2560.

16. Chen J, Jo S, and P. K., *Degradable hydrogels.* Handbook of biodegradable polymers, 1997 p. 203–230.

17. Joyce Y. Wong, J.D.B., *Biomaterials*. 2007, CRC Press: NY.

18. Anseth, K.S., C.N. Bowman, and L. BrannonPeppas, *Mechanical properties of hydrogels and their experimental determination.* Biomaterials, 1996. **17**(17): p. 1647-1657.

19. Kopecek, J. and J.Y. Yang, *Revie - Hydrogels as smart biomaterials.* Polymer International, 2007. **56**(9): p. 1078-1098.

20. Brandl, F., F. Sommer, and A. Goepferich, *Rational design of hydrogels for tissue engineering: Impact of physical factors on cell behavior.* Biomaterials, 2007. **28**(2): p. 134-146.

21. Gong, J.P., et al., *Double-network hydrogels with extremely high mechanical strength.* Advanced Materials, 2003. **15**(14): p. 1155-+.

22. Orwin, E.J., M.L. Borene, and A. Hubel, *Biomechanical and optical characteristics of a corneal stromal equivalent.* Journal of Biomechanical Engineering-Transactions of the Asme, 2003. **125**(4): p. 439-444.

23. Petrini, P., et al. *Design, synthesis and properties of polyurethane hydrogels for tissue engineering*. 2003.

24. M. Ahearne, Y. Yang, and K.-K. Liu, *Mechanical Characterization of Hydrogels for Tissue Engineering.* Applications Topics in Tissue Engineering, 2008. **4**.

25. Okumura, Y. and K. Ito, *The polyrotaxane gel: A topological gel by figure-of-eight cross-links.* Advanced Materials, 2001. **13**(7): p. 485-+.

26. Haraguchi, K. and T. Takehisa, *Nanocomposite hydrogels: A unique organic-inorganic network structure with extraordinary mechanical, optical, and swelling/de-swelling properties.* Advanced Materials, 2002. **14**(16): p. 1120-1124.

27. Schexnailder, P. and G. Schmidt, *Nanocomposite polymer hydrogels.* Colloid and Polymer Science, 2009. **287**(1): p. 1-11.

28. Mu, J.F. and S.X. Zheng, *Poly(N-isopropylacrylamide) nanocrosslinked by polyhedral oligomeric silsesquioxane: Temperature-responsive behavior of hydrogels.* Journal of Colloid and Interface Science, 2007. **307**(2): p. 377-385.

29. Paxton, J.Z., et al., *Engineering the Bone-Ligament Interface Using Polyethylene Glycol Diacrylate Incorporated with Hydroxyapatite.* Tissue Engineering Part A, 2009. **15**(6): p. 1201-1209.

30. Peyton, S.R., et al., *The use of poly(ethylene glycol) hydrogels to investigate the impact of ECM chemistry and mechanics on smooth muscle cells.* Biomaterials, 2006. **27**(28): p. 4881-4893.

31. Jang, H.N., Y.B. Chung, and S.S. Kim, *Preparation and Characterization of Silicone Hydrogel Lens Containing Poly(ethylene glycol).* Polymer-Korea, 2009. **33**(2): p. 169-174.

32. Iza, M., et al., *Hydrogels of poly(ethylene glycol): mechanical characterization and release of a model drug.* Journal of Controlled Release, 1998. **52**(1-2): p. 41-51.

33. Hern, D.L. and J.A. Hubbell, *Incorporation of adhesion peptides into nonadhesive hydrogels useful for tissue resurfacing.* Journal of Biomedical Materials Research, 1998. **39**(2): p. 266-276.

34. Hu, B.H., J. Su, and P.B. Messersmith, *Hydrogels Cross-Linked by Native Chemical Ligation.* Biomacromolecules, 2009. **10**(8): p. 2194-2200.

35. Hennink, W.E. and C.F. van Nostrum, *Novel crosslinking methods to design hydrogels.* Advanced Drug Delivery Reviews, 2002. **54**(1): p. 13-36.

36. C.Decker, *PHOTOINITIATED CROSSLINKING POLYMERISATION.* Prog. Polym Sci, 1996. **21**: p. 593-650.

37. Tranchida, D. and S. Piccarolo, *Relating morphology to nanoscale mechanical properties: from crystalline to mesomorphic iPP.* Polymer, 2005. **46**(12): p. 4032-4040.

38. Instron. *Wilson Instruments Hardness Testers* 2009 07/20 [cited 2009 07/20].

39. Liu, X. and V. Piotter, *Mapping micro-mechanical properties of carbon-filled polymer composites by TPM.* Precision Engineering-Journal of the International Societies for Precision Engineering and Nanotechnology, 2007. **31**(2): p. 162-168.

40. Crosby, A.J. and J.Y. Lee, *Polymer nanocomposites: The "nano" effect on mechanical properties.* Polymer Reviews, 2007. **47**(2): p. 217-229.

41. Klapperich, C., K. Komvopoulos, and L. Pruitt, *Nanomechanical properties of polymers determined from nanoindentation experiments.* Journal of Tribology-Transactions of the Asme, 2001. **123**(3): p. 624-631.

42. Ebenstein, D.M. and L.A. Pruitt, *Nanoindentation of soft hydrated materials for application to vascular tissues.* Journal of Biomedical Materials Research Part A, 2004. **69A**(2): p. 222-232.

43. Lee, S.Y., et al., *Unconfined compression properties of a porous poly(vinyl alcohol)-chitosan-based hydrogel after hydration.* Acta Biomaterialia, 2009. **5**(6): p. 1919-1925.

44. Tsang, V.L. and S.N. Bhatia, *Three-dimensional tissue fabrication.* Advanced Drug Delivery Reviews, 2004. **56**(11): p. 1635-1647.

45. Discher, D.E., P. Janmey, and Y.L. Wang, *Tissue cells feel and respond to the stiffness of their substrate.* Science, 2005. **310**(5751): p. 1139-1143.

46. Levental, I., P.C. Georges, and P.A. Janmey, *Soft biological materials and their impact on cell function.* Soft Matter, 2007. **3**(3): p. 299-306.

47. Solon, J., et al., *Fibroblast adaptation and stiffness matching to soft elastic substrates.* Biophysical Journal, 2007. **93**(12): p. 4453-4461.

48. Wilder, E.A., et al., *Measuring the modulus of soft polymer networks via a buckling-based metrology (vol 39, pg 4138, 2006).* Macromolecules, 2006. **39**(17): p. 5956-5956.

49. Dimitriadis, E.K., et al., *Determination of elastic moduli of thin layers of soft material using the atomic force microscope.* Biophysical Journal, 2002. **82**(5): p. 2798-2810.

50. Cheng, Y.T. and C.M. Cheng. *What is indentation hardness?* 2000.

51. Li, X.D. and B. Bhushan, *A review of nanoindentation continuous stiffness measurement technique and its applications.* Materials Characterization, 2002. **48**(1): p. 11-36.

52. Franke, O., et al., *Mechanical properties of hyaline and repair cartilage studied by nanoindentation.* Acta Biomaterialia, 2007. **3**(6): p. 873-881.

53. Kim, J.J., et al., *Nanocrystallization during nanoindentation of a bulk amorphous metal alloy at room temperature.* Science, 2002. **295**(5555): p. 654-657.

54. Hengsberger, S., A. Kulik, and P. Zysset, *Nanoindentation discriminates the elastic properties of individual human bone lamellae under dry and physiological conditions.* Bone, 2002. **30**(1): p. 178-184.

55. Michel, J.P., et al., *Nanoindentation studies of full and empty viral capsids and the effects of capsid protein mutations on elasticity and strength.* Proceedings of the National Academy of Sciences of the United States of America, 2006. **103**(16): p. 6184-6189.

56. Ebenstein, D.M. and L.A. Pruitt, *Nanoindentation of biological materials.* Nano Today, 2006. **1**(3): p. 26-33.

57. Haque, F., *Application of nanoindentation to development of biomedical materials.* Surface Engineering, 2003. **19**(4): p. 255-268.

58. Schuh, C.A., *Nanoindentation studies of materials.* Materials Today, 2006. **9**(5): p. 32-40.

59. Golovin, Y., *Nanoindentation and mechanical properties of solids in submicrovolumes, thin near-surface layers, and films: A Review.* Physics of the Solid State, 2008. **50**(12): p. 2205-2236.

60. Briscoe, B.J., L. Fiori, and E. Pelillo, *Nano-indentation of polymeric surfaces.* Journal of Physics D-Applied Physics, 1998. **31**(19): p. 2395-2405.

61. Kaufman, J.D., et al., *Time-dependent mechanical characterization of poly(2-hydroxyethyl methacrylate) hydrogels using nanoindentation and unconfined compression.* Journal of Materials Research, 2008. **23**(5): p. 1472-1481.

62. Binnig, G., C.F. Quate, and C. Gerber, *ATOMIC FORCE MICROSCOPE.* Physical Review Letters, 1986. **56**(9): p. 930-933.

63. Hinterdorfer, P. and Y.F. Dufrene, *Detection and localization of single molecular recognition events using atomic force microscopy.* Nature Methods, 2006. **3**(5): p. 347-355.

64. Dufrene, Y.F., *Using nanotechniques to explore microbial surfaces.* Nature Reviews Microbiology, 2004. **2**(6): p. 451-460.

65. Garcia, R. and R. Perez, *Dynamic atomic force microscopy methods.* Surface Science Reports, 2002. **47**(6-8): p. 197-301.

66. Jalili, N. and K. Laxminarayana, *A review of atomic force microscopy imaging systems: application to molecular metrology and biological sciences.* Mechatronics, 2004. **14**(8): p. 907-945.

67. Domke, J. and M. Radmacher, *Measuring the elastic properties of thin polymer films with the atomic force microscope.* Langmuir, 1998. **14**(12): p. 3320-3325.

68. Lin, D.C. and F. Horkay, *Nanomechanics of polymer gels and biological tissues: A critical review of analytical approaches in the Hertzian regime and beyond.* Soft Matter, 2008. **4**(4): p. 669-682.

69. Kaufman, J.D. and C.M. Klapperich, *Surface detection errors cause overestimation of the modulus in nanoindentation on soft materials.* Journal of the Mechanical Behavior of Biomedical Materials, 2009. **2**(4): p. 312-317.

70. Constantinides, G., et al., *Probing mechanical properties of fully hydrated gels and biological tissues.* Journal of Biomechanics, 2008. **41**(15): p. 3285-3289.

71. Liu, K.F., M.R. VanLandingham, and T.C. Ovaert, *Mechanical characterization of soft viscoelastic gels via indentation and optimization-based inverse finite element analysis.* Journal of the Mechanical Behavior of Biomedical Materials, 2009. **2**(4): p. 355-363.

72. Alkorta, J., J.M. Martinez-Esnaola, and J.G. Sevillano, *Critical examination of strain-rate sensitivity measurement by nanoindentation methods: Application to severely deformed niobium.* Acta Materialia, 2008. **56**(4): p. 884-893.

73. G, B., et al., Phys. Rev. Lett. , 1983. **50**: p. 120.

74. Cappella, B. and G. Dietler, *Force-distance curves by atomic force microscopy.* Surface Science Reports, 1999. **34**(1-3): p. 1-+.

75. Butt, H.J., B. Cappella, and M. Kappl, *Force measurements with the atomic force microscope: Technique, interpretation and applications.* Surface Science Reports, 2005. **59**(1-6): p. 1-152.

76. Harmon, M.E., D. Kucking, and C.W. Frank, *Photo-cross-linkable PNIPAAm copolymers. 5. Mechanical properties of hydrogel layers.* Langmuir, 2003. **19**(26): p. 10660-10665.

77. Pharr, G.M. and W.C. Oliver, *MEASUREMENT OF THIN-FILM MECHANICAL-PROPERTIES USING NANOINDENTATION.* Mrs Bulletin, 1992. **17**(7): p. 28-33.

78. Oliver, W.C. and G.M. Pharr, *Measurement of hardness and elastic modulus by instrumented indentation: Advances in understanding and refinements to methodology.* Journal of Materials Research, 2004. **19**(1): p. 3-20.

79. Yang, N., et al., *Frequency-dependent viscoelasticity measurement by atomic force microscopy.* Measurement Science & Technology, 2009. **20**(2).

80. Tagit, O., N. Tomczak, and G.J. Vancso, *Probing the morphology and nanoscale mechanics of single poly(N-isopropylacrylamide) microgels across the lower-critical-solution temperature by atomic force microscopy.* Small, 2008. **4**(1): p. 119-126.

81. Derjaguin, B.V., V.M. Muller, and Y.P. Toporov, *EFFECT OF CONTACT DEFORMATIONS ON ADHESION OF PARTICLES.* Journal of Colloid and Interface Science, 1975. **53**(2): p. 314-326.

82. Johnson, K.L., K. Kendall, and A.D. Roberts, *SURFACE ENERGY AND CONTACT OF ELASTIC SOLIDS.* Proceedings of the Royal Society of London Series a-Mathematical and Physical Sciences, 1971. **324**(1558): p. 301-&.

83. Bykov, V., A. Gologanov, and V. Shevyakov, *Test structure for SPM tip shape deconvolution.* Applied Physics a-Materials Science & Processing, 1998. **66**(5): p. 499-502.

84. Gibson, C.T., et al., *Calibration of AFM cantilever spring constants.* Ultramicroscopy, 2003. **97**(1-4): p. 113-118.

85. Yang, C.W., et al., *Imaging of soft matter with tapping-mode atomic force microscopy and non-contact-mode atomic force microscopy.* Nanotechnology, 2007. **18**(8): p. 8.

86. Cappella, B. and D. Silbernagl, *Nanomechanical properties of polymer thin films measured by force-distance curves.* Thin Solid Films, 2008. **516**(8): p. 1952-1960.

87. Belov, A.N., et al. *TEST STRUCTURE FOR SPM TIP SHAPE DECONVOLUTION*. in *International Conference on Physics, Chemistry and Application of Nanostructures*. 2009. Minsk, RUSSIA: World Scientific Publ Co Pte Ltd.

88. Ghosh, K., et al., *Cell adaptation to a physiologically relevant ECM mimic with different viscoelastic properties.* Biomaterials, 2007. **28**(4): p. 671-679.

89. Myung, D., et al., *Biomimetic strain hardening in interpenetrating polymer network hydrogels.* Polymer, 2007. **48**(18): p. 5376-5387.

90. Stefan Gäbler, J.S., Thomas Koch, Sabine Seidler, Georg Schüller, H. Redl, *Determination of the viscoelastic properties of hydrogels based on polyethylene glycol diacrylate (PEG-DA) and human articular cartilage.* Int. J. Materials Engineering Innovation, 2009. **1**(1).

91. Wilder, E.A., et al., *Measuring the modulus of soft polymer networks via a buckling-based metrology.* Macromolecules, 2006. **39**(12): p. 4138-4143.

92. Levy, R. and M. Maaloum, *Measuring the spring constant of atomic force microscope cantilevers: thermal fluctuations and other methods.* Nanotechnology, 2002. **13**(1): p. 33-37.

93. Calabri, L., et al., *AFM nanoindentation: tip shape and tip radius of curvature effect on the hardness measurement.* Journal of Physics-Condensed Matter, 2008. **20**(47).

Vita

Zouheir Drira is from Tunis, Tunisia. Zouheir completed his Bachelor of Science with a major in chemistry and minor in mathematics from Murray State University. He started his graduate studies in chemical and life engineering at Virginia Commonwealth University in Fall 2007.